A new stegosaurian dinosaur (Ornithischia: Thyreophora) with a remarkable dermal armour from the Middle Jurassic of North Africa

Omar Zafaty, Mostafa Oukassou, Facundo Riguetti, Julio Company, Saad Bendrioua, Rodolphe Tabuce, André Charrière, Xabier Pereda-Suberbiola

▶ **To cite this version:**

Omar Zafaty, Mostafa Oukassou, Facundo Riguetti, Julio Company, Saad Bendrioua, et al.. A new stegosaurian dinosaur (Ornithischia: Thyreophora) with a remarkable dermal armour from the Middle Jurassic of North Africa. Gondwana Research, 2024, 131, pp.344-362. 10.1016/j.gr.2024.03.009 . hal-04781064

HAL Id: hal-04781064
https://hal.science/hal-04781064v1

Submitted on 14 Nov 2024

HAL is a multi-disciplinary open access archive for the deposit and dissemination of scientific research documents, whether they are published or not. The documents may come from teaching and research institutions in France or abroad, or from public or private research centers.

L'archive ouverte pluridisciplinaire **HAL**, est destinée au dépôt et à la diffusion de documents scientifiques de niveau recherche, publiés ou non, émanant des établissements d'enseignement et de recherche français ou étrangers, des laboratoires publics ou privés.

Gondwana Research 131 (2024) 344–362

A new stegosaurian dinosaur (Ornithischia: Thyreophora) with a remarkable dermal armour from the Middle Jurassic of North Africa

Omar Zafaty[a], Mostafa Oukassou[a,*], Facundo Riguetti[b], Julio Company[c], Saad Bendrioua[d], Rodolphe Tabuce[e], André Charrière[f], Xabier Pereda Suberbiola[g]

[a] Hassan II University of Casablanca, Laboratory of Applied Geology, Geoinformatics and Environment, Department of Geology, Faculty of Sciences Ben M'sick, Morocco
[b] Universidad Maimónides & CONICET, Fundación de Historia Natural Félix de Azara Centro de Ciencias Naturales Ambientales y Antropológicas, Hidalgo 775, 7th floor (PC: 1405) Buenos Aires, Argentina
[c] Universitat Politècnica de València, Departamento de Ingeniería del Terreno, 46022 Valencia, Spain
[d] Moulay Ismail University, Laboratory of Geoscience, Geodynamics and Georesources, Faculty of Sciences, Meknès, Morocco
[e] Montpellier University, Institut des Sciences de l'Evolution, UMR5554, CNRS, IRD, EPHE, Montpellier, France
[f] Toulouse III University, 13 Terrasses de la Figuière, 30140 Anduze, France
[g] Universidad del País Vasco/Euskal Herriko Unibertsitatea, Facultad de Ciencia y Tecnología, Departamento de Geología, Apdo. 644, 48080 Bilbao, Spain

[*] Corresponding author.
E mail address: mostafa.oukassou@univh2c.ma (M. Oukassou).

Abstract

In recent years the Middle Atlas of Morocco has become an area of interest for the study of dinosaurs in northern Africa. The Boulahfa locality, near Boulemane, has produced a diverse dinosaur assemblage from the Middle Jurassic of the El Mers Group. Fossil remains of sauropods and thyreophorans, such as ankylosaurs (*Spicomellus*) and stegosaurs (*Adratiklit*), have been reported so far in this region. Here, we describe a new partial thyreophoran skeleton found in the gray marls of the El Mers III Formation (Bathonian-?Callovian), which mainly consists of disarticulated dorsal vertebrae and ribs, and associated dermal armour elements. Axial characters (e.g., elongated pedicels of the dorsal neural arches; upturned transverse processes and dorsal ribs with straight axes suggesting a narrow ribcage) indicate that the specimen belongs to a medium to large sized stegosaur. The dorsal vertebrae show differences with those of *Adratiklit*, whose material has been found at the same stratigraphic levels. *Thyreosaurus atlasicus* gen. et sp. nov. is characterized by a remarkable dermal armour, which consists of thick (up to 4 cm) subovate to subrectangular shaped osteoderms. The asymmetrical texture of their sides, one roughly ornamented with small pits and fiber bundles, the other with a well marked cross hatched pattern, is clearly different from that observed to date in other stegosaurs (and ankylosaurs). The bone histology of these osteoderms is reminiscent of that of stegosaurian tail spines. It is interpreted that these osteoderms were arranged in a recumbent position over the body of the animal, instead of an erect position. The holotype corresponds to an adult individual who did not reach its maximum body size (estimated body length 6 m). The phylogenetic analysis suggests that *Thyreosaurus* is closely related to *Dacentrurus* within Dacentrurinae. The recent discoveries of *Adratiklit* and *Thyreosaurus* provide insight into the early evolution of stegosaurs in the Middle Jurassic of Africa.

1. Introduction

Thyreophora is a diverse clade of herbivorous ornithischian dinosaurs composed of stegosaurs, ankylosaurs, and basal forms (Norman et al., 2004). Thyreophorans have an extensive fossil record,

spanning from the Lower Jurassic to the Upper Cretaceous, which is best known from well preserved specimens in Laurasia. In contrast, fossil remains are poorly known and mostly partial in Gondwana (see Maidment et al., 2020; Soto Acuña et al., 2021; Riguetti et al., 2022a and references). In Africa, thyreophorans could have been present since the Early Middle Jurassic (Ridgwell and Sereno, 2010). Stegosaurian body fossils are documented in the Middle Jurassic of Morocco (*Adratiklit*; Maidment et al., 2020), the Upper Jurassic of Tanzania (*Kentrosaurus*; Hennig, 1915, 1925; Galton, 1982) and the Lower Cretaceous of South Africa (*Paranthodon*; Galton and Coombs, 1981; Raven and Maidment, 2018). African ankylosaurs are represented only by *Spicomellus* afer from the Middle Jurassic of Morocco (Maidment et al., 2021).

Important dinosaur sites are known in the Atlas Mountains of Morocco (Lapparent, 1955; Monbaron et al., 1999, Allain et al.,2004; Maidment et al., 2020, 2021). In recent decades, the Middle Atlas region has become an important focus area for the study of Mesozoic vertebrates, especially the Boulemane El Mers region, which is rich in dinosaur bones, eggs and footprints. The first dinosaur skeletal fossils were found in the Middle Jurassic (El Mers I Formation) sites of this area (Termier et al., 1940; Lapparent, 1955; Dresnay, 1963), including sauropod ('*Cetiosaurus mogrebiensis*'; Lapparent, 1955; Upchurch and Martin, 2003) and theropod remains ('*Megalosaurus mersensis*'; Lapparent, 1955; may be a teleosaurid crocodyliform; see Chabli, 1985; Carrano et al., 2012). In the Middle Jurassic continental deposits (Charrière and Haddoumi, 2016) of this area (El Mers Group), thyreophorans have been described recently from the El Mers III Formation near Boulemane. These include the stegosaur *Adratiklit boulahfa* (Maidment et al., 2020), the first thyreophoran described from North Africa, and the ankylosaur Spicomellus afer (Maidment et al., 2021), a bizarre armoured dinosaur with spiked dermal armour fused to the dorsal surface of the ribs.

The Middle Atlas region hosts also numerous ichnological sites mentioned since the 1930s (Termier, 1936; Jenny et al., 1981); however, these sites were not described until the early 2000s, first by Meyer and Thüring (2004,2005) and subsequently by Hadri and Lorente (2012) at the El Mers localities, which included sauropod and non avian theropod tracks from the Middle Jurassic (Bathonian-?Callovian). The Boulahfa locality near Boulemane also yielded a few isolated tracks comprising a sauropod manus pes set and a small stegosaurian pes imprint (cf. *Stegopodus*) from the Upper Jurassic or Lower Cretaceous Oued El Atchane Formation (Oukassou et al., 2023). Additionally, diverse dinosaur eggshell remains have been described from the Upper Cretaceous (Maastrichtian) deposits of this area (Garcia et al., 2003; Vianey Liaud and Garcia, 2003).

In 2021, during a geological mapping mission south of Boulemane, three of the authors (OZ, MO and SB) discovered a new site rich in dinosaur remains in the El Mers III Formation. This site, named Boulahfa North, is located north of the Boulahfa quarry (Charroud and Fedan, 1992). The material was collected over several consecutive field trips, and consists of a partial postcranial skeleton of a stegosaur that includes dorsal vertebrae and ribs, a limb bone and dermal armour. The aims of this paper are i) to describe the new specimen, which is proposed as the holotype of a new stegosaurian genus and species; ii) to compare the material with that of *Adratiklit* and other stegosaurs; and iii) to analyze the phylogenetical position of the new taxon. Finally, this study aims to contribute to a better understanding of the diversity of Jurassic thyreophorans from North Africa.

Institutional abbreviations
HIIUC, Hassan II University of Casablanca, Casablanca, Morocco;
BN, Boulahfa North.

2. Geological setting

The Middle Atlas constitutes the northeastern segment of the Moroccan Atlas system (Fig. 1), an intracontinental belt erected during the Alpine orogeny in relation to the development of the Atlantic Ocean and the Western Tethys (Frizon de Lamotte et al., 2008; Escosa et al., 2021). During the Triassic, the area was an active rift basin (Ouarhache, 2002). Early stages of rifting were accompanied by the deposition of evaporitic continental facies and the setting up of effusive and then explosive

tholeiitic basalts (Ouarhache et al., 2012), followed by deposition from the Liassic to the Bajocian (Benshili, 1989) of a thick transgressive sequence of deep marine marls and shallow marine carbonates. Middle Jurassic (Bathonian-?Callovian) deposits are composed of regressive sequences of shallow marine and continental mixed clastic, evaporitic and carbonate sediments (Charrière, 1990; Fedan, 1993).

In this regressive context, different Middle Atlas basins have recorded considerable variations in the sedimentation of the El Mers Group deposits (Charrière et al., 2011; Pratt et al., 2015). Subsequently, the area was subjected to an extended period of erosion and coarse terrestrial clastic sedimentation (?Late Jurassic ?Early Cretaceous). Later, the transgressive Barremian Aptian sequence marks the outbreak of the Cretaceous Paleogene cycle (Charrière, 1996).

The El Mers Group (Bathonian-?Callovian) is divided into three formations known as El Mers I, II and III. South of Boulemane, the El Mers I Formation consists of dolomitic beds rich in dinosaur footprints and emersion structures followed by varicolored marls rich in dinosaur bones (Lapparent, 1955) alternating with freshwater limestones, evolving to coastal sandstones (sandy limestones and coquina beds). The El Mers II Formation is composed up of a thick coastal sandy limestone series. The El Mers III Formation, which has provided the fossil remains described here (Fig. 1C), is represented by a series of many tens of meters (~60 m) of fine friable gray marls, green pinkish marls and siltstones interspersed with calcareous marls (Fig. 2A). At the base of the series, siltstones are organized into irregular pinkish and greenish laminae (Fig. 2D) bearing sauropod footprints (Fig. 2E). This deformed level laterally changes to greenish gray marls rich in fossil wood (Fig. 2F), dinosaur bones (Fig. 2H), and pyrite concretions indicating a continental sedimentary environment with reducing conditions. At the top, the marls are locally interspersed with small lenses of poorlygraded sandstones and, dolomitic limestones covered, through an erosional unconformity, by sedimentary breccia, paleochannel sandstones and conglomerates of the Oued El Atchane Formation (Fig. 2C) and pinky siltstones with root traces (rhizolites) (Fig. 2G), indicating a paleosol.

3. Materials and methods

The fossil site HIIUC BN was discovered in rocks of the El Mers III Formation in the northern Boulahfa locality, near Boulemane, Middle Atlasof Morocco (GPS coordinates: 33.320520°N; 4.712273°W). The quarry map, drawn during the excavation of the fossil remains is reproduced in Fig. 3. The collected material is composed of a stegosaurian disarticulated partial skeleton consisting of dorsal vertebrae and ribs, a limb bone (fibula?) and dermal bones. All these remains were found disarticulated but associated within a small area (approximately 3 square meters). Therefore, they most likely belong to a single individual.

HIIUC BN was prepared using small airscribes, dental tools, and brushes. Cleaning was performed exclusively by using water and paper towels. Polyvinyl acetate dissolved in acetone was applied as a consolidant, and cyanoacrylate and two part epoxy were used as adhesives. After preparation, measurements were made by hand and from scaled photographs taken with a Nikon® D300s camera (AF NIKKOR 50 mm 1:1.8 D lens) using Adobe® Illustrator CC©. A complete list of the examined specimens and measurements are summarized in Table 1.

The photogrammetric 3D models were created from photos involving multiple cameras capture whose positions were recorded. MeshLab software was used to create 3D models from a point cloud generated by Agisoft Metashape Professional software. The constructed 3D models make it possible to simultaneously study the material, highlighting the greatest possible detail, and making it accessible to other researchers online.

For the study of the bone tissue structure, transverse histological thin sections were produced from two osteoderms (HIIUC BN14 and 15) and a dorsal rib (HIIUC BN25). The fossils were sampled and prepared according to the methodology outlined by Chimsamy and Raath (1992) and posteriorly developed by Lamm (2013). Thin sections were prepared from slices taken transversally to one of the sets of fiber bundles that ornament the osteoderm surface, if possible, including the edge of the osteoderm where the ornamentation changes from dorsal to ventral. The resulting histological

preparations were examined under normal and polarized light, using a transmitted light polarizing microscope Olympus® BXTR BX40 connected to a digital camera Sony® CybershotTM QX 100. The digital images obtained were processed with Adobe® PhotoshopTM CC. The nomenclature and definitions of bone histology used are mainly based on Francillon Vieillot et al. (1990), Reid (1996) and subsequent works. For the osteoderms, we largely follow the terminology proposed by Scheyer and Sander (2004).

A phylogenetic analysis was performed to test the relationships of the new material. We include the new taxon in the dataset of Dai et al. (2022); modified from Maidment et al. (2020). It now consists of 27 taxa and 115 characters (both quantitative and morphological characters). Characters 1–24, 105 and 106 were treated as additive. No character was weighted. *Pisanosaurus* was fixed as the outgroup taxon. The analysis was performed in TNT v.1.5 (Goloboff and Catalano, 2016). A New Technology search was carried using 10 RAS (random addition sequences) of the Sectorial Search, Tree Fusing, Ratchet and Drift algorithms. To the recovered most parsimonious trees (MPT), a resampling with TBR (Tree bisection reconnection) was made. Branch support was calculated with 1.000 pseudoreplicates of Bootstrap resampling (Traditional search) and 1000 replicates of Symmetrical resampling (Traditional search).

The fossil remains are permanently housed in the collections of the Department of Geology, Ben M'sick Faculty of Sciences, Hassan II University of Casablanca, Morocco.

4. Results

4.1. Systematic paleontology

Dinosauria Owen, 1842. Ornithischia Seeley, 1888. Stegosauria Marsh, 1877.

Thyreosaurus atlasicus gen. et sp. nov.

Etymology: Generic name *Thyreosaurus* from ''thyreos" (Ancient Greek: htqeó1), an oblong shield that was used by Hellenistic armies and later adopted by other peoples; a reference to the osteoderms of the specimen, and ''saurus" (Ancient Greek: raũqo1), which means lizard. The specific name *atlasicus* refers to the Atlas Mountains of Morocco and North Africa.

Holotype: HIIUC BN00, a partial postcranial skeleton that includes 9 dorsal vertebrae and 21 dorsal rib remains, a limb bone (fibula?), and six dermal elements. These remains are interpreted as belonging to a single individual.

Horizon and locality: Boulahfa North, central Middle Atlas, Morocco; El Mers III Formation, Middle Jurassic, Bathonian-?Callovian (Charrière et al., 2011).

Diagnosis: Differs from all other stegosaurs in having thick osteoderms that are suboval to subrectangular in shape, with an asymmetrical texture: one side is irregularly ornamented and bears small pits, and the other surface is ornamented with a cross hatched pattern; the arrangement of the dermal elements is assumed to be recumbent rather than erect.

Thyreosaurus differs from *Dacentrurus* and *Adratiklit* in the smaller overall dimensions of the dorsal centra relative to the neural arch. Moreover, the autapomorphies described for the other stegosaur found in the El Mers III Formation, *Adratiklit* (anteriorly projecting rugosities related to the anterior centroparapophysial laminae on either side of the neural canal in dorsal vertebrae and small, triangular, rugose protuberance situated dorsally on the prezygapophyses posterior to the articular facets), are absent in *Thyreosaurus*.

4.2. Description

4.2.1. Dorsal vertebrae

Nine dorsal vertebrae are known (Figs. 4–6). Two of them are almost complete, with the centrum and much of the neural arch, including the diapophyses and the neural spine (HIIUC BN01,

03); four vertebrae preserve the centrum and an incomplete neural arch (the neural spine is missing) (HIIUC BN02, 05, 06, 07); two specimens preserve only parts of the neural arch (HIIUC BN04, 08), and one shows only a fragmentary centrum (HIIUC BN09). In general, the fossils are well preserved, although some specimens show evidence of diagenetic deformation (especially the HIIUCBN03 vertebra, which displays a deformed centrum and a displaced diapophysis).

Four of the centra are wider transversely than long anteroposteriorly (Figs. 5A, B, 4A, B), but in two vertebrae (HIIUC BN03, 07) the centrum length exceeds the lateromedial width (Fig. 6A, B). The centrum width is equal to slightly greater than the centrum height in almost all vertebrae, except in HIIUC BN07, which is higher than wide (could be due to deformation) (Fig. 6B). Both articular facets of the centra are flat (amphiplatyan) to slightly concave. The borders of the articular facets are well defined. In anterior and posterior views, the centra have a subcircular or heart shaped outline. The lateral sides of the centra are anteroposteriorly concave and slightly convex dorsoventrally. The anterior articular facet is more ventrally projected than the posterior facet in two of the centra (HIIUC BN01, 02) (Fig. 5). In the ventral view, the centra are spool shaped. A distinct keel is present on the ventral surface of all the centra. The neurocentral suture is apparently not visible, suggesting a non juvenile ontogenetic state for the individual.

The neural arch is dorsally elongated; the height of the neural arch is at least 2.5 greater than that of the centrum (HIIUC BN01, 03) (Figs. 5A, 6A). In HIIUC BN01, the neural arch pedicels are much narrower above the neural canal than in other vertebrae and show a great widening above towards the diapophyses (Fig. 5A).

The neural canal is rather small, oval to subtriangular in outline, higher than wide. In HIIUC BN05, the height of the neural canal exceeds half the height of the neural arch from its base (junction with the centrum) to the basal part of the prezygapophyses (Fig. 4A). In HIIUC BN02 and HIIUC BN03, the neural canal is almost half the height (Figs. 5B, 6A). Finally, in HIIUC BN01 the neural canal is small and subcircular, with a ratio of approximately a quarter of the neural arch height (Fig. 5A). In HIIUC BN02, the neural canal is larger on its anterior side than on its posterior side (Fig. 5B). On the top of the HIIUC BN01 neural canal there is a marked bony roof, especially on the posterior side (Fig. 5A).
The parapophyses are situated at the level or just below the prezygapophyses at the base of the diapophyses. The parapophyses are slightly elliptical in shape and are arranged obliquely backwards (Figs. 4–6).

In anterior view, the prezygapophyses are situated high relative to the neural canal (HIIUC BN01 to HIIUC BN04) (Figs. 5, 6A, 4C). In HIIUC BN03, the prezygapophyses are large and face dorsomedially (Fig. 6Aa). The articular surfaces are oval in outline. They are joined ventrally to form a V shaped articulation surface. The prezygapophyses are oriented at an angle of approximately 100° to each other. In the lateral view, they extend further anteriorly than the anterior border of the centrum. The neural arch forms an intraprezygapophyseal shelf between the prezygapophyses. The area posterior to the prezygapophyses shows a midline depression that is backed posteriorly by a vertical sheet bearing a midline ridge that continues dorsally with the neural spine (Figs. 5, 4C). The prezygapophyses are welded to the rest of the neural arch on both sides in HIIUC BN03 (Fig. 6A), but separated by a very shallow notch posterior to the left prezygapophysis in HIIUC BN07 (Fig. 6B). In both cases, prezygapophyses are horizontally oriented in the lateral view.

The articular surfaces of the postzygapophyses are flat and slightly oval in outline. In posterior view, the postzygapophyses face ventrolaterally and are separated by a midline groove; this groove may be open ventrally (HIIUC BN01, 03, 04) (Figs. 5A, 6A, 4C) or closed (HIIUC BN02, 08) (Figs. 5B, 6C). A prominent ridge extends along the midline from the base of the postzygapophyses to the dorsal margin of the neural canal (HIIUCBN01 to HIIUC BN05) (Figs. 5, 6A, 4A C). On both sides of this ridge, there is a shallow fossa. In lateral view, the postzygapophyses extend beyond the level of the posterior surface of the centrum (HIIUC BN01 and especially HIIUC BN03, but this extension is probably due in part to deformation) (Figs. 5A, 6A).

The transverse processes are dorsoventrally compressed and broad anteroposteriorly in dorsal view, mainly HIIUC BN03 (Fig. 6A), whose section is flat (while in other vertebrae it is triangular). The transverse processes project dorsolaterally at an angle of approximately 120 130° from each other

(barely 100° in HIIUC BN05) (Fig. 4A). When preserved, the diapophyses do not reach the level of the top height of the neural spine (HIIUC BN01, 02, 04; deformed in HIIUC BN03) (Figs. 5, 6A, 4C).

The presence of centroparapophyseal laminae (acpl, pcdl; terminology of Wilson, 1999) cannot be confirmed in the dorsal vertebrae. HIIUC BN05 exhibits a short process below the parapophyses, but this process is located in the middle part of the pedicels of the neural arch and does not have continuity, so it does not reach the anterior lateral margin of the neural canal (Fig. 4A).

The neural spine is a transversely compressed plate that is slightly wider at the top (HIIUC BN01, 03, 08 and especially HIIUC BN04) (Figs. 5A, 6A, C). The thickness of the neural spine is greater at the front than at the back. It is well projected dorsally (the posterodorsal projection in HIIUC BN03 is due to deformation), its height being equivalent or slightly greater than that of the centrum (HIIUC BN01, 03) (Figs. 5A, 6A). In lateral view, the anterior edge of the neural spine is slightly convex, while the posterior one is straight or very slightly concave. Therefore, its general shape is comparable to that of the tip of a blunt scimitar. The anteroposterior length of the spine is greater at the base than at the top. The height/anteroposterior length ratio of the neural spine is approximately 1.5–2 mm (Figs. 5A, 6A, 4C, 6C). Finally, there is no evidence of ossified epaxial tendons associated with the dorsal vertebrae.

4.2.2. Dorsal ribs

Twenty one dorsal rib remains are known (UIIUC BN18 to 38). Three of them are relatively complete (HIIUC BN18, 20 and 21) (Fig. 7A C D) and the remainders are more fragmentary. Four ribs preserve the capitulum tuberculum (HIIUC BN20 to 23) (Fig. 7C DE F) and two preserve only the tuberculum (HIIUC BN26, 27). Other more fragmentary dorsal ribs are identified as proximal (HIIUC BN25, 28) or distal fragments (HIIUC BN30 38) (Supplementary data). The specimens are generally well preserved, but four ribs show evidence of fracture and/or taphonomic deformation (HIIUC BN18, 19, 21, 24) (Fig. 7A B D G).

In anterior or posterior view, the dorsal ribs are gently curved ventromedially along their length. The capitulum is an elongate, finger like process, which is much more developed than the tuberculum. The capitulum projects from the proximal part of the shaft at an angle ranging from 100° to 130°. The articular surface of the capitulum is elliptical and elongated; that of the tuberculum is also elliptical with well defined edges. The rib shaft is anteroposteriorly compressed proximally. The anterior surface of the shaft is concave and shows a prominent ridge forming a low flange that extends ventrally. In the proximal cross section, the ribs are T shaped. Then, they become subtriangular and gradually the section becomes oval shaped towards the middle part of the shaft, and transversely compressed and blade like distally. The distal end of the rib (only preserved in HIIUC BN18, 30, 32) is very slightly expanded. (Fig. 7A; Supplementary data).

4.2.3. Appendicular bone

Only one appendicular bone is known in the assemblage. It is a slender, rod like and rather straight bone, with a slightly expanded (distal?) end. The shaft is oval in cross section, with a convex side and a flat side. It shows a thick, prominent ridge in the proximal (?) part. Due to its poor preservation, the identification of this element and comparisons with other stegosaurs are problematic, although this could correspond to an incomplete fibula (Supplementary data).

4.2.4. Dermal armor

Six dermal elements of different sizes have been identified (HIIUC BN11 16) (Figs. 8–10AA). The larger osteoderms HIIUCBN11 and HIIUC BN12 were found closely associated at the site, and not far from HIIUC BN13, HIIUC BN14 and HIIUC BN16 (see arrow 3 in Fig. 3B). HIIUC BN15 was discovered next to the dorsal vertebra HIIUC BN01 (see arrow 4 in Fig. 3B).

Although incomplete, HIIUC BN11 is the largest dermal element, with dimensions of 31.7 x 27 cm as preserved (maximum thickness of 3.4 cm) (Fig. 8). Considering the preserved natural edges, it could be a subovate to subrectangular shaped plate. It shows a quite asymmetrical texture. One (concave) side is roughly ornamented, with an irregular, non homogeneous surface where small pits

and fibrous bundles are visible (Fig. 8B). Additionally, some small parts of this surface may be devoid of ornamentation and are rather smooth. The other (convex) side is wavy and exhibits a homogeneously ornamented surface, with a cross hatched pattern of fibers at angles between 90° and 120° (Fig. 8A). This cross hatched pattern varies in size; the interweaving is smaller toward the edges, while in the center it is coarser. In the wavy surfaces, this pattern becomes curved instead of straight. Near the natural edges, longitudinal fibers dominate instead of the cross hatched pattern. As shown by the fractured areas, the osteoderm thickness is greater in the center than at the edges. Two edges bear rugosities or indentations (Fig. 8C D).

HIIUC BN12 is also an osteoderm of relatively large dimensions (25.9 x 15.2 cm as preserved), although with apparently more rounded edges (suboval to subromboidal in outline?) (Fig. 9A). The same asymmetry is observed in HIIUC BN11, namely one concave side with an irregular surface made of pits and fibrous bundles (Fig. 9Ad) and the other with a wavy, homogeneous surface with an interwoven pattern of longitudinal fibers arranged at right angles (Fig. 9Ab).

HIIUC BN13 is a nearly complete plate of intermediate size (17 x 12.2 cm) (Fig. 9B). It is rather flat (2.4 cm) and has a subrect angular outline. A slightly convex side shows small foramina and fiber bundles (Fig. 9Bd). The slightly concave side is ornamented with pits and an interwoven pattern of fibers, which are arranged forming an angle of about 120° (Fig. 9Bb). As occurs in the larger plates, near the edges the cross hatched pattern is replaced by longitudinal fibers. The natural edges have a rugose surface, with indentations and foramina (Fig. 9Ba,c,e,f).

Other osteoderms are smaller in size (HIIUC BN14, HIIUC BN15, HIIUC BN16). They exhibit an asymmetrical texture, with an irregular side showing longitudinal fiber bundles and rugose edges and the other side is an ornamented surface with a cross hatched pattern. In HIIUC BN15 (12 x 7 cm, maximum thickness 2.3 cm), the irregular surface is slightly convex while the ornamented surface with a cross fibrous tissue is flat to barely concave (Fig. 10A). The thickness is greater on the inside (2.3 cm) than on the edge (0.7 cm). HIIUC BN16 is a small, oval osteoderm (8.9 x 4.8 cm)
(Fig. 9C). The surface with pits and fibrous bundles is flat; the surface with the cross hatched pattern of longitudinal fibers is convex. Finally, HIIUC BN14 is a fragmentary osteoderm (5 x 3 cm as preserved, maximum thickness 4 cm) that does not preserve any natural edge (Fig. 10A).

4.3. Histology

4.3.1. Osteoderms

As mentioned above, two fragmentary osteoderms (HIIUC BN14 and HIIUC BN15) were selected for the histological study. The histological descriptions are mainly based on the specimen HIIUC BN15, since this osteoderm has suffered a lower degree of secondary remodeling.

Histological sections show that both osteoderms show a massive and compact (i.e., dense) structure (Fig. 10A–C). The original extension of the external cortices is largely diminished by the expansion of the internal cancellous core. Trabecular bone represent between 90 % and 95 % (HIIUC BN15) and almost 100 % (HIIUC BN14) of the osteoderm thickness. When present, the transition from the cortical bone to the internal cancellous core is marked by the massive occurrence of dense Haversian bone and resorption cavities (Fig. 10D).

The scarce non remodeled, primary cortex is restricted, as much, near to the outer surface of the osteoderms. When occurs, consists of primary woven fibered bone composed of large mineralized collagen fiber bundles with longitudinal simple primary vascular canals (Fig. 10D E). These intrinsic fibers (interwoven structural fiber bundles: Scheyer and Sander, 2004) are arranged in orthogonal sets and form an interwoven mat like fabric. Primary osteons are rare in the cortex. In the specimen HIIUC BN14 several closely spaced lines of arrested growth occur in the outermost cortex. Some bundles of Sharpey's fibers occur, exhibiting an oblique alignment with the osteoderm surface.

The internal cancellous region of the osteoderms (i.e., the core) is dominated by thick trabecular bone composed mostly by a mixture of secondary tissues with evidence of extensive erosionreconstruction cycles: dense cancellous bone with large resorption cavities lined by thick layers of centripetally deposited lamellar bone, and densely packed secondary osteons, forming patches of

dense Haversian bone. Remnants of primary tissues, mainly composed of randomly distributed structural fibers of woven bone, occur in interstitial areas of the trabecula (Fig. 10C).

A striking characteristic of both osteoderms is the extensive remodeling of the primary bone tissues by secondary reconstruction, giving the osteoderms a ‘‘non fibrous” bone appearance. Such substantial degree of secondary remodeling is not usual in ankylosaurian or even in titanosaurian osteoderms, but has been described in dorsal plates and tail spines of ontogenetically adult stegosaurs (Main et al., 2005; Hayashi et al., 2009, 2012). As commented above, the external cortices are much obliterated by secondary remodeling, but, when present, they consist of interwoven bundles of mineralized collagen fibers. Similar meshworks of orthogonal fiber bundles have been documented in the cortices of osteoderms of basal archosauriforms (Cerda et al., 2013), in ankylosaurian osteoderms (Scheyer and Sander, 2004; Hayashi et al., 2010; Burns and Currie, 2014), in dermal ossicles of titanosaurs (Cerda and Powell, 2010), and in dermal bones of xenarthran mammals (Wolf et al., 2012), but not in plates or in tail spikes of stegosaurs (Hayashi et al., 2012). According to general consensus, this kind of fibrous tissue is originated by metaplastic ossification of pre existing connective tissues (Haines and Mohuiddin, 1968, Scheyer and Sander, 2004; Main et al., 2005; Cerda and Powell, 2010; Vickaryous and Hall, 2008; Hayashi et al., 2012). Therefore, the primary compact bone of the osteodermal cortices is considered here as metaplastic in origin.

Given the presence of lines of arrested growth (LAGs) and the great development of the secondary remodeling, which increases with age, the dermal bones of the holotype of *Thyreosaurus* can be referred to an individual of advanced ontogenetic stage (OS3: young adult to old adult) proposed for Stegosaurus by Hayashi et al., (2009,2012).

4.3.2. Dorsal rib

A fragmentary rib (HIIUC BN25) was also selected for histological analysis. The fragment corresponds, approximately, to the proximal most one third of the bone, lacking the tuberculum and capitulum processes. The rib fragment was cross sectioned both proximally and distally, making use of the existence of broken ends. The proximal section, noticeably robust, was particularly interesting in order to obtain the thickest cortex possible and, therefore, the maximal growth record. Nevertheless, as this part of the bone resulted heavily remodeled, most of the histological information comes from the study of the distalmost section of the recovered shaft.

The distalmost section of the rib fragment shows a relatively narrow compact cortex, surrounding a large medullary cavity completely filled with a dense trabecular network of cancellous bone (Fig. 11A). Enlarged resorption cavities from the perimedullary region extend up to the outer cortex producing, in certain areas, the trabecularisation of the compacta (perimedullar bone remodeling: Francillon Viellot et al., 1990).

The areas or the cortex not invaded by medullar drift preserve the original primary bone tissue. According to the bone histology described for Stegosaurus ribs (Hayashi et al., 2009), the primary cortex consists of a well vascularized fibrolamellar bone, with longitudinal and circular vascular canals arranged in a laminar vascularity (Fig. 11B). The vascular density does not reduce noticeably towards the outer cortex. In the outermost cortex, some of the vascular spaces of the primary osteons remain incompletely filled by lamellar tissue, indicating that the osteonal deposition has not finished (Fig. 11B). At least six cortical growth marks are preserved in the compacta (i.e., lines of arrested growth or LAGs), giving the cortex the appearance of a zonal bone (Fig. 11B). The distribution of these rest lines in the cortex seems fairly irregular, and do not decrease in spacing towards the bone periphery. Some of them are double and triple LAGs, making it difficult to estimate the total LAG count. The expansion of the medullary region and the intense secondary remodeling in the innermost cortex by secondary osteons has probably obliterated one or more of the earliest deposited LAGs. The mid cortex only exhibits the presence of randomly scattered, incompletely filled secondary osteons (Fig. 11B). No secondary osteons invade the outermost cortex.

It is now widely accepted that a well vascularized bone matrix composed of fibro lamellar bone is correlated with rapid bone deposition in fast growing, somatically immature animals (Amprino, 1947; Francillon Vieillot et al, 1990; Stokstad, 2004; Bailleul et al., 2019; Padian and Woodward, 2021).

Since the vascularity density did not reduces dramatically in the outer cortex, and there is neither the presence of slowly deposited tissues in the periphery of the bone (e.g., parallel fiber or lamellar bone) nor subperiosteal structures of cessation of growth correlated with old ages (the so called external fundamental system, EFS), and according to the osteoderm histology, the rib bone histology also suggests that the holotype specimen of *Thyreosaurus atlasicus* was an adult but not skeletally mature animal, actively growing at the time of death.

4.4. Phylogenetic analysis

The phylogenetic analysis recovered one MPT with a length of 269.67. The strict consensus (Fig. 12) shows the same topology to that of Dai et al. (2022) with *Thyreosaurus* recovered within the Dacentrurinae. The position of *Thyreosaurus* as the sister taxon of *Dacentrurus* is well supported, with values similar to those of the clade Stegosaurus (Fig. 12). The synapomorphies recovered for Dacentrurinae include the derived states of the characters 11, 12 and 61. The characters 11 and 12 (quantitative) refer to the dimensions of the distal humeral width relative to both the lesser humeral width of diaphysis ratio (character 11) and humeral length (character 12). The distal end of the humerus shows a gradual decreasing along the tree, with the minimum values within Dacentrurinae (node reconstruction: char. 11 = 1.92; char. 12 = 0.32). This character is not coded in *Thyreosaurus*. The other synapomorphy of Dacentrurinae is the presence of dorsal centra wider than long (present in *Thyreosaurus*). In fact, this feature was tradicionally used to diagnose *Dacentrurus* (Galton, 1985; Maidment et al., 2008). A recent study also shows that wide centra in the caudal vertebrae are also diagnostic of the Dacentrurinae (Costa and Mateus, 2019).

5. Discussion

5.1. Comparisons and taxonomic comments

Based on the morphological characters of the described vertebrae and ribs and their comparison with those of complete skeletons of stegosaurs (e.g., *Stegosaurus stenops*; Maidment et al., 2015), most of the dorsal region, except for the most posterior dorsal vertebrae and ribs, seems to be represented in HIIUC BN00. Nine dorsal vertebrae are preserved in the HIIUC BN assemblage; 13 to 16 dorsal vertebrae are commonly present in stegosaurs (Maidment et al., 2015; Maidment and Pereda Suberbiola, in press). Considering several features (e.g., prezygapophyses inclination; parapophyses position relative to the prezygapophyses; neural canal size; centrum length; diapophyses inclination; neural arch pedicel elongation) we can approach the approximate placement of the dorsal vertebrae in *Thyreosaurus*. Vertebrae HIIUCBN05, 06 and probably HIIUC BN04 belong to the anteriormost dorsals (1–3), while HIIUC BN01 03 and HIIUC BN07 are middorsal vertebrae (between the 5–10 positions, comparable to the holotype of *Adratiklit*).

The dorsal vertebrae show a combination of characters that is typical of stegosaurs, such as, prezygapophyses fused on the midline, elongation of the pedicel region above the neural canal, and upturned transverse processes (Galton and Upchurch, 2004; Maidment et al., 2008). Moreover, the dorsal ribs have straight axes, suggesting that the shape of the ribcage is narrow and taller than it is wide, as commonly observed in stegosaurs (see Mallison, 2010 for *Kentrosaurus*).

Most of the dorsal centra of *Thyreosaurus* are wider than long, as occurs in *Adratiklit*, *Dacentrurus*, *Hesperosaurus* and *Miragaia*, and in contrast to other stegosaurs, such as *Huayangosaurus*, *Kentrosaurus*, *Loricatosaurus* and *Stegosaurus*, in which the dorsal centra are longer than they are wide (see Hennig, 1925; Zhou, 1984; Galton, 1985, 1990; Maidment et al., 2008, 2015, 2020; Costa and Mateus, 2019 and references). However, in HIIUC BN03 and HIIUC BN07 the centra are slightly longer than wide. Also, the overall dimensions of the dorsal centra relative to the neural arch in *Thyreosaurus* are smaller than in *Dacentrurus* (Galton, 1985) and *Adratiklit* (Maidment et al., 2020).

The dorsal neural arch pedicles of *Thyreosaurus* (mainly HIIUCBN01 and HIIUC BN03) are more elongated above the neural canal than in the dorsal vertebrae of *Bashanosaurus* (Dai et al., 2022), and *Huayangosaurus* (Zhou, 1984; Maidment et al., 2006), but not as strongly elongated above the neural canal as in *Kentrosaurus* (Hennig, 1925; Galton, 1982), *Loricatosaurus* (Galton, 1985 as *Lexovisaurus*) and some specimens of *Stegosaurus* (Ostrom and McIntosh, 1999). HIIUC BN02 bears a neural arch slightly shorter than HIIUC BN01 and HIIUC BN03, and resembles the anterior dorsal vertebrae of *Dacentrurus* (Galton, 1985) and *Miragaia* (Costa and Mateus, 2019).

Thyreosaurus clearly differs from *Kentrosaurus* and *Huayangosaurus* in that the neural canal is not as dorsally expanded (see Hennig, 1925; Galton, 1982; Zhou, 1984). It differs from *Hesperosaurus* and *Chungkingosaurus* in having a dorsal neural spine that is only slightly higher than the diapophyses, whereas in these genera it is much higher (Carpenter et al., 2001). Moreover, it differs from *Chungkingosaurus* in the amphiplatyan condition of the dorsal centra, whereas in the latter the anterior articular facet is strongly convex (Maidment et al., 2018). *Thyreosaurus* is different from *Giantspinosaurus* in the absence of deep central fossae on the lateral surfaces of the dorsal centra (Dai et al., 2022) and from *Stegosaurus* in the presence of a prominent notch ventrally between the postzygapophyses (Galton and Upchurch, 2004; Dai et al., 2022).

The dorsal vertebrae of *Thyreosaurus* resemble at first glance those of *Adratiklit*. However, the two autapomorphies described by Maidment et al. (2020) for *Adratiklit* cannot be identified in HIIUC BN. There is no evidence of anterocentroparapophysial laminae (ACPL) that extends anteriorly forming rugose processes on either side of the neural canal, nor of a small, triangular, rugose protuberance situated dorsally on the prezygapophyses posterior to the articular facets. It should be noted that the presence of ACPL is variable in stegosaurs, with differences due to ontogeny and even differences within the vertebral series of the same individual (see Maidment et al., 2015 for individual variation in Stegosaurus stenops). Besides, the triangular protuberance has only been observed in a left prezygapophysis of the holotype specimen of *Adratiklit* boulahfa (Maidment et al., 2020: Fig. 8c), and similar structures seem to be present in other stegosaurs (see Hennig, 1925; Galton, 1982; Maidment et al., 2015).

Another difference is probably associated with the mentioned protuberance of the prezygapophysis. Along the dorsal series in Stegosaurus (Maidment et al., 2015), *Kentrosaurus* (Hennig, 1925; Galton, 1982) and *Hesperosaurus* (Carpenter et al., 2001), and an isolated vertebrae of *Adratiklit* (Maidment et al., 2020), *Loricatosaurus* (Galton, 1985), and *Tuojiangosaurus* (Dong et al., 1977), prezygapophyses are anterodorsally directed in lateral view, and are separated from the diapophyses by a deep notch in both lateral and dorsal views. However, the prezygapophyses of *Thyreosaurus* bear a horizontal orientation in lateral view and are posteriorly continued with the diapophyses through a continuous prezygodiapophyseal lamina, both lacking or bearing a subtle (not deep) notch in both lateral and dorsal views. A similar condition seems to occur in *Huayangosaurus* (Zhou, 1984; Maidment et al., 2006), Bashanosaurus (Dai et al., 2022) and probably *Omosaurus lenieri* (Nopcsa, 1911; *Dacentrurus* for Maidment et al., 2008).

Other differences observed between *Thyreosaurus* and *Adratiklit* are the following: the dorsal centra of *Adratiklit* are more constricted laterally than in HIIUC BN and thus more pronounced spool shaped in ventral view; the absence of a distinct keel on the ventral surface of the dorsal centra in *Adratiklit* (a ventral keel is present only in the cervical centra, as commonly in stegosaurs); the location of the (obliterated) suture is marked by an anteroposterior ridge in *Adratiklit*, whereas the neurocentral suture is apparently not visible in *Thyreosaurus*; the intraprezygapophyseal shelf is much narrower in *Adratiklit*; the postzygapophyses extend posteriorly to about the same level as the posterior surface of the centrum in *Adratiklit*, whereas in *Thyreosaurus* they extend well beyond the level of the posterior centrum surface. Although it cannot be definitively excluded that these differences are due to individual variation or taphonomic deformation, we consider that at least some of them (for instance, the presence of a ventral keel in all dorsal centra and the absence of a deep notch between prezygapophyses and diapophyses) are significant enough to differentiate *Thyreosaurus* from *Adratiklit*.

Furthermore, the dorsal vertebrae from the Boulahfa North site are comparatively larger in size than those of *Adratiklit*. Considering the dorsal series of *Stegosaurus* (Maidment et al., 2015), the dorsal vertebrae of *Thyreosaurus* are similar to slightly larger, suggesting a medium to large sized stegosaur (estimate body length 6 m).

The osteoderms are the most remarkable elements of the new stegosaur. Although variable in size (between 5 and more than 30 cm in length), they are unique among thyreophorans in having an asymmetrical ornamentation, with one side showing an irregular surface with small pits and fiber bundles, while the other is characterized by an interlocking weave texture (Fig. 10B). A cross fibered texture was documented in the base of the osteoderms of several non stegosaurian thyreophorans, including the ankylosaurs *Antarctopelta* (Ricqlès et al., 2001; F.R. pers. obs.), *Edmontonia* (Hayashi et al., 2010), *Glyptodonpelta* (Burns, 2008), *Patagopelta* (Riguetti et al., 2022b), *Polacanthus* (Blows, 2015), and the basal form *Scelidosaurus* (Norman, 2020). On the other hand, stegosaurian plates bear a symmetrical texture on both sides, consisting of a rugose and pitted base, irregular flat, lateral surfaces provided with vascular grooves (mostly of apicobasal direction) in most of the plate, and a frayed texture with deep furrows towards the distal edges (Gilmore, 1914; Hayashi et al., 2012). Therefore, the asymmetric ornamentation in *Thyreosaurus* suggests a recumbent orientation of the plates, with the side strongly ornamented with a cross fibered texture as the ventral side.

Histological evidence also supports this interpretation. The base of the stegosaurian plates is the main growing region of the plate (besides some cortical bone growing in the whole osteoderm surface), bearing some secondary remodeling, large vascular networks and fiber bundles (metaplastic bone) that represent attachment sites for Sharpey's fibers of the dermal tissues in life and held the plate in an erect position (Buffrénil et al., 1986; Hayashi et al., 2009, 2012). In the osteoderms of *Thyreosaurus*, the presence of fiber bundles transversal to the osteoderm surface only in one side of the plate supports a different orientation over the body of the new stegosaur (see '4.3 Histology', above). These fibers are associated to the side of the plate that shows the cross fibered ornamentation. Considering the age and probable phylogenetic relations of *Thyreosaurus*, the available material for comparisons is scarce. Stegosaurian fossils from the Middle Jurassic and dacentrurine skeletons preserve few remains of osteoderms and most of them are fragmentary (e.g., Galton, 1985, 1990; Escaso et al., 2007; Mateus et al., 2009; Costa and Mateus, 2019; Dai et al., 2022). Most of the osteoderms are composed of almost complete dermal spines and fragmentary bases of dermal plates. However, in all cases there are elements that show a bilateral symmetry suggesting a vertical placement over the body of the stegosaur in life, contrasting with the recumbent placement of the osteoderms in *Thyreosaurus*. Until finding more complete and/or articulated stegosaurian skeletons, this feature is considered diagnostic of *Thyreosaurus*. However, due to the poor osteoderm record, the presence of recumbent plates in other related stegosaurs cannot be ruled out.

Osteoderms different from the typically stegosaurian erect plates and/or spines are common in non stegosaurian thyreophorans, including scutes, bosses, ossicles, shields, etc. (see Blows, 2015). Few stegosaurs bear some of these osteoderms, like scutes in *Huayangosaurus* and gular ossicles in *Stegosaurus* (Gilmore, 1914; Sereno and Dong, 1992; Hayashi et al., 2014; Maidment et al., 2015). In Huayangosaurus, there are recorded several scutes in the thoracic region of an articulated individual (Zhou, 1984) that resemble the scutes present in most non stegosaurian thyreophorans. This represents a plesiomorphic feature for Stegosauria. In another way, the derived position of *Thyreosaurus* supports the recumbent disposition of the osteoderms as an autapomorphy of this taxon.

5.2. Phylogenetic and paleobiogeographical implications for Gondwanan stegosaurs

Both Moroccan stegosaurs were recovered as Dacentrurinae, allowing some phylogenetic and paleobiogeographic implications. On one hand, both skeletons are very incomplete, suggesting unstable terminals a priori. However, both stegosaurs are recovered within the Dacentrurinae, and *Thyreosaurus* with a strong branch support, comparable to that of the clade formed by *Stegosaurus stenops* and *S. homheni*. Also, the character 61 (dorsal centra wider than long) is strong enough to

retain the Moroccan taxa within the same clade. It is worth noting that the anatomical differences between *Adratiklit* and *Thyreosaurus* are also reflected in the topology, since both taxa collected from the same geological formation were not recovered as sister taxa. In this way, the Middle Atlas of Morocco would exhibit part of the early diversification of stegosaurs during the Middle Jurassic. Since only a few characters were codded for both species, results must be taken with caution in the light of more findings to get a strongly supported topology for the analysis of the diversity of Moroccan stegosaurs.

On the other hand, the finding of *Thyreosaurus* and *Adratiklit* as independent dacentrurine taxa has also a paleobiogeographical importance. The early diversification of stegosaurs during the Middle Jurassic is represented by taxa from Argentina, China, England, France and Morocco. Besides the Argentinian *Isaberrysaura* and the Chinese *Bashanosaurus*, which are basal stegosaurs, *Loricatosaurus* from England and France, and both Moroccan taxa, are recovered as derived stegosaurs. This suggest that the diversification of Late Jurassic stegosaurs begins early, at least during the Middle Jurassic. Also, the presence of both basal stegosaurs in Argentina and older members of Dacentrurinae in North Africa shows an increase in the importance of Gondwanan taxa regarding the early stages of the stegosaurian evolution. Until recent years, the origin and evolution of early stegosaurs was considered to have occurred in Eastern Asia (Dong, 1990). However, several recent findings in Africa and South America (Maidment et al., 2020, 2021; Rauhut et al., 2020; Riguetti et al., 2022a) show that early thyreophorans had not only a more extensive distribution since their origin, but also that Gondwanan taxa had an important role in the evolution of both thyreophorans and eurypodans.

6. Conclusions

The thyreophoran dinosaur *Thyreosaurus* atlasicus gen. et sp. nov. is described here on the basis of postcranial remains found in the Middle Atlas Mountains south of Fès, Morocco. The continental gray marls of the Bathonian-?Callovian El Mers III Formation at Boulahfa North fossil site near Boulemane have yielded the partial skeleton of a single individual, which mainly includes dorsal vertebrae and ribs, together with a set of osteoderms, belonging to a medium to large sized stegosaur (estimate body length 6 m). The presence of abundant bone remodeling in the cortex and of cyclical growth marks suggest that the material belongs to an adult, but not fully skeletal mature individual. The dermal elements of *Thyreosaurus* are suboval to subrectangular shaped plates of variable size (from 10 to more than 30 cm in length). They are considered unique for their robustness and thickness (up to 4 cm), and due to the fact that they exhibit an asymmetrical ornamentation: one of the sides has small pits and fiber bundles, while the other (regarded as ventral) is characterized by showing a marked cross hatched surface. Anatomical and histological approaches support that these osteoderms were not arranged erect but rather recumbent on the dorsum of the animal in life. The nature and orientation of these osteoderms appear highly unusual and are therefore different from those known to date for stegosaurs.

After *Adratiklit* boulahfa (Maidment et al., 2020), *Thyreosaurus* atlasicus is the second stegosaur described from the Middle Jurassic of Morocco. This discovery shows that the diversity of African stegosaurs during the Jurassic was higher than previously thought and emphasizes the presence of unsuspected dermal elements among stegosaurs.

The phylogenetic analysis suggests that *Thyreosaurus* is a member of Dacentrurinae and supports previous interpretation of Moroccan stegosaurs as more closely related to *Dacentrurus* from Europe than to other African stegosaurs such as *Kentrosaurus* and Paranthodon. In addition, the recent findings testify of the early diversification of stegosaurs during the Middle Jurassic and highlights the role played by the Gondwanan continents in the evolution of thyreophorans.

Finally, this research emphasizes the importance of the fossil sites from the Middle Atlas of Morocco for understanding the evolutionary history of Gondwanan dinosaurs and, more particularly, the African thyreophorans.

CRediT authorship contribution statement

Omar Zafaty: Conceptualization, Data curation, Writing – original draft. Mostafa Oukassou: Conceptualization, Data curating, Writing – reviewing & editing. Facundo Riguetti: Data curation, Writing – reviewing & editing. Julio Company: Conceptualization, Writing – reviewing & editing. Saad Bendrioua: Data curation. Rodolphe Tabuce: Writing – reviewing & editing. André Charrière: Writing – reviewing & editing. Xabier PeredaSuberbiola: Conceptualization, Writing – reviewing & editing.

Acknowledgments

The authors would like to thank the editor J. Meert, the reviewer Dr. S. Hayashi and the other anonymous reviewer, whose comments greatly improved the manuscript. The Oukassou family is warmly thanked for their hospitality during the excavation mission. The faculty of Sciences Ben M'sick, Hassan II University of Casablanca, kindly provided logistical support during field trips. This project has been funded by the Ministry of Europe and Foreign Affairs (MEAE), the Ministry of Higher Education, Research (MESR) and the Ministry of Higher Education, Scientific Research and Innovation (MESRSI), under the framework of the Franco Moroccan bilateral program PHC TOUBKAL 2023, with Grant number: 12345AB. Research of JC and XPS is financed by the Spanish Ministry of Science and Innovation (MCIN) and the European Regional Development Fund (FEDER) (research project PID2021 122612OB I00); research of XPS is also financed by the Basque Country Government (research group IT1485 22).

Supplementary material

Supplementary data to this article can be found online at https://doi.org/10.1016/j.gr.2024.03.009.

References

Allain, R., Aquesbi, N., Dejax, J., Meyer, C., Monbaron, M., Montenat, C., Taquet, P., 2004. A basal sauropod dinosaur from the Early Jurassic of Morocco. Comptes Rendus Palevol, 3(3), 199-208.

Amprino, R., 1947. La structure du tissu osseux envisagée comme expression de différences dans la vitesse de l'accroissement. Arch Biol. 58, 315-330.

Arbour, V.M., Currie, P.J., 2016. Systematics, phylogeny and palaeobiogeography of the ankylosaurid dinosaurs. J. Syst. Palaeontol. 14, 385-444. https://doi.org/10.1080/14772019.2015.1059985

Blows, W.T., 2015. British polacanthid dinosaurs. Observations on the history and palaeontology of the UK Polacanthid Armoured Dinosaurs and their relatives. Siri Scientific Press, 220p.

Burns, M.E., Currie, P.J., 2014. External and internal structure of ankylosaur (Dinosauria; Ornithischia) osteoderms and their systematic relevance. J. Vertebr. Paleontol. 34, 835–851. https://doi.org/10.1080/02724634.2014.840309

Buffrénil, V.de., Farlow, J.O., Ricqlès, A.de., 1986. Growth and function of *Stegosaurus* plates: evidence from bone histology. Paleobiology 12, 459-473. https://doi.org/10.1017/S0094837300003171.

Burns, M.E., 2008. Taxonomic utility of ankylosaur (Dinosauria, Ornithischia) osteoderms: *Glyptodontopelta mimus* Ford, 2000: a test case. J. Vertebr. Paleontol. 28(4), 1102-1109. https://doi.org/10.1671/0272-4634-28.4.1102.

Carpenter, K, Miles, C.A., Cloward, K., 2001. New primitive stegosaur from the Morrison Formation of Wyoming. In: Carpenter K, ed. The Armored dinosaurs. Bloomington: Indiana University Press, 55-75.

Carrano, M.T., Benson, R.B., Sampson, S.D., 2012. The phylogeny of Tetanurae (Dinosauria: Theropoda). J. Syst. Palaeontol. 10(2), 211-300. https://doi.org/10.1080/14772019.2011.630927.

Cerda, I.A., Powell, J.E., 2010. Dermal armor histology of *Saltasaurus loricatus*, an Upper Cretaceous sauropod dinosaur from northwest Argentina. Acta Palaeontol. Pol. 55, 389-398. http://dx.doi.org/10.4202/app.2009.1101

Cerda, I.A., Desojo, J.B., Scheyer, T.M., Schultz, C.L., 2013. Osteoderm microstructure of "rauisuchian" archosaurs from South America. Geobios 46, 273–283. https://doi.org/10.1016/j.geobios.2013.01.004

Chabli, S., 1985. Données nouvelles sur un "Dinosaurien" jurassique moyen du Maroc: *Megalosaurus mersensis* Lapparent 1955, et sur les Megalosauridés en général. In : Les Dinosaures de la Chine à la France. Colloque international de paléontologie, Toulouse, 65-72.

Charrière, A., 1990. Héritage hercynien et évolution géodynamique alpine d'une chaîne intracontinentale : Le Moyen-Atlas au SE de Fès. (Maroc). Thèse Etat, Univ. Paul Sabatier, 589p.

Charrière, A., Haddoumi, H., 2016. Les "Couches rouges" continentales jurassico-crétacées des Atlas marocains (Moyen Atlas, Haut Atlas central et oriental): bilan stratigraphique, paléogéographies successives et cadre géodynamique. Bol. Geol. Min. 127(2-3), 407-430.

Charrière, A., Ouarhache, D., El Arabi, H., 2011. Le Moyen Atlas (Middle Atlas). In Michard et al (eds.), Nouveaux guides géologiques et miniers du Maroc. Notes & Mém. Serv. Géol. Maroc 559, 11-164.

Charroud, M., Fedan, B., 1992. Données préliminaires sur la découverte du gisement de Boulahfa à dinosauriens (SW de Boulemane, Moyen Atlas central). In Livre à la mémoire de Georges Choubert. Le Maroc promontoire africain entre la Méditerranée et l'Atlantique. Notes & Mém. Serv. Géol. Maroc 366: 448-449.

Chimsamy, A., Raath, M.A., 1992. Preparation of fossil bone for histological examination. Palaeontol. Africana 29, 39-44.

Costa, F., Mateus, O., 2019. Dacentrurine stegosaurs (Dinosauria): A new specimen of *Miragaia longicollum* from the Late Jurassic of Portugal resolves taxonomical validity and shows the occurrence of the clade in North America. PLoS One 14(11), e0224263. https://doi.org/10.1371/journal.pone.0224263.

Dai, H., Li, N., Maidment, S.C.R., Wei, G., Zhou, Y., Hu, X., Ma, Q., Wang, X., Hu, H., Peng, G., 2022. New stegosaurs from the Middle Jurassic Lower Member of the Shaximiao Formation of Chongqing, China. Journal of Vertebrate Paleontology 41(5), e1995737. https://doi.org/10.1080/02724634.2021.1995737.

Dong, Z.M., 1990. Stegosaurs of Asia. In Carpenter, K. and Currie, P.J. Dinosaur Systematics: Approaches and perspectives. Cambridge University Press, Cambridge. 255–268.

Dresnay, R.du., 1963. Données stratigraphiques complémentaires sur le Jurassique moyen des synclinaux d'El Mers et de Skoura (Moyen Atlas, Maroc). Bulletin de la Société Géologique de France 7(6), 883-900. https://doi.org/10.2113/gssgfbull.S7-V.6.883.

Escaso, F., Ortega, F., Dantas, P., Malafaia, E., Silva, B., Sanz, J.L., 2007. Elementos postcraneales de *Dacentrurus* (Dinosauria: Stegosauria) del Jurásico Superior de Moçafaneira (Torres Vedras, Portugal). Cantera Paleontológica 157, 172.

Escosa, F.O., Leprêtre, R., Spina, V., Gimeno-Vives, O., Kergaravat, C., Mohn, G., de Lamotte, D.F., 2021. Polyphased mesozoic rifting from the Atlas to the north-west Africa paleomargin. Earth-Sci. Rev. 220, 103732. https://doi.org/10.1016/j.earscirev.2021.103732 .

Francillon-Vieillot, H., de Buffrénil, V., Castanet, J., Géraudie, J., Meunier, F.J., Sire, J.-Y., Zylberberg, L., de Ricqlès, A., 1990. Microstructure and mineralisation of vertebrate skeletal tissues. In: Carter, J.G. (Ed.), Skeletal Biomineralisation: Patterns, Processes and Evolutionary Trends, I. Van Nostrand Reinhold, pp. 471-530.

Frizon de Lamotte, D., Zizi, M., Missenard, Y., Hafid, M., El Azzouzi, M., Maury, R.C., Charrière, A., Taki, Z., Benammi, M., Michard, A., 2008. The Atlas system. In Michard, A., Saddiqi, O., Chalouan, A., Frizon de Lamotte, D. (Eds.), Continental evolution: The Geology of Morocco. Lect. Notes Earth Sci. 116, 33-202. https://doi.org/10.1007/978-3-540-77076-3_4.

Galton, P.M., 1982. The postcranial anatomy of stegosaurian dinosaur *Kentrosaurus* from the Upper Jurassic of Tanzania, East Africa. Geol. Palaeontol. 15, 139-160.

Galton, P.M., 1985. British plated dinosaurs (Ornithischia, Stegosauridae). J. Vertebr. Paleontol. 5(3), 211-254. https://doi.org/10.1080/02724634.1985.10011859.

Galton, P.M., 1990. A partial skeleton of the stegosaurian dinosaur *Lexovisaurus* from the uppermost Lower Callovian (Middle Jurassic) of Normandy, France. Geol. Palaeontol. 24, 185-199.

Galton, P.M., Coombs, W.P., 1981. *Paranthodon africanus* (Broom) a stegosaurian dinosaur from the Lower Cretaceous of South Africa. Geobios 14(3), 299-309. https://doi.org/10.1016/S0016-6995(81)80177-5.

Galton, P. M., Upchurch, P., 2004. Stegosauria. In Weishampel, D.B., Dodson, P., Osmólska, H. (eds.), The Dinosauria. University of California Press, Berkeley. second edition, 343-362.

Garcia, G., Tabuce, R., Cappetta, H., Marandat, B., Bentaleb, I., Benabdallah, A., Vianey-Liaud, M., 2003. First record of dinosaur eggshells and teeth from the North-West African Maastrichtian (Morocco). Paleovertebrata 32, 59-69.
Gilmore, C.W., 1914. Osteology of the armored Dinosauria in the United States National Museum, with special reference to the genus *Stegosaurus*. Bull. U. S. Natl. Mus. 89, 1-143.

Goloboff, P.A., Catalano, S.A., 2016. TNT version 1.5, including a full implementation of phylogenetic morphometrics. Cladistics 32(3), 221-238. https://doi.org/10.1111/cla.12160.

Hadri, M., & Lorente, F. P., 2012. Historia de yacimientos con huellas de dinosaurio, desde su descubrimiento hasta su primer estudio: alrededores de El Mers (Marruecos). Zubia, (30), 93.

Haines, R.W., Mohuiddin. A., 1968. Metaplastic bone. J. Anat. 103, 527-538.

Hayashi, S., Carpenter, K., Suzuki, D., 2009. Different growth patterns between the skeleton and osteoderms of *Stegosaurus* (Ornithischia: Thyreophora). J. Vertebr. Paleontol. 29, 123–131. https://doi.org/10.1080/02724634.2009.10010366

Hayashi, S., Carpenter, K., Scheyer, T.M., Watabe, M., Suzuki, D., 2010. Function and evolution of ankylosaur dermal armor. Acta Palaeontol. Pol. 55, 213–228. https://doi.org/10.4202/app.2099.0103

Hayashi, S., Carpenter, K., Watabe, M., McWhinney, L., 2012. Ontogenetic histology of *Stegosaurus* plates and spikes. Palaeontology 55, 145-161. https://doi.org/10.1111/j.1475-4983.2011.01122.x

Hayashi, S., Redelstorff, R., Mateus, O., Watabe, M., Carpenter, K., 2014. Gigantism of stegosaurian osteoderms. J. Vertebr Paleontol. Program and Abstracts 2014, 145.

Hennig, E., 1915. *Kentrosaurus aethiopicus*, der Stegosauride des Tendaguru. Sitzungsber. Gesell. naturf. Freunde Berlin, 1915, 219-247.

Hennig, E., 1925. *Kentrurosaurus aethiopicus*. Die Stegosaurier-Funde vom Tendaguru, Deutsch-Ostafrika. Palaeontographica, 2 Suppl. 7, 101-254.

Jenny, J., Le Marrec, A., & Monbaron, M., 1981. Les empreintes de pas de dinosauriens dans le Jurassique moyen du Haut Atlas central (Maroc): nouveaux gisements et précisions stratigraphiques. Geobios, 14(3), 427-431.

Lamm, E.T., 2013. Preparation and sectioning of specimens. In: Padian, K., Lamm E.T., (Eds.), Bone histology of fossil tetrapods: advancing methods, analysis and interpretation. University of California Press, pp. 55-160.

Lapparent, A.F. de., 1955. Etude paléontologique des vertébrés du Jurassique d'El Mers (Moyen Atlas). Notes & Mém. Serv. Géol. Maroc 124, 1-36.

Maidment, S.C., Pereda-Suberbiola, X., in press. Basal Thyreophora and Stegosauria. In: The Dinosauria, 3rd edition. Cambridge University Press.

Maidment, S.C., Wei, G., Norman, D.B., 2006. Re-description of the postcranial skeleton of the Middle Jurassic stegosaur *Huayangosaurus taibaii*. Journal of Vertebrate Paleontology 26(4), 944-956. https://doi.org/10.1671/0272-4634(2006)26[944:ROTPSO]2.0.CO;2.

Maidment, S.C., Norman, D.B., Barrett, P.M., Upchurch, P., 2008. Systematics and phylogeny of Stegosauria (Dinosauria: Ornithischia). J. Syst. Palaeontol. 6(4), 367-407. https://doi.org/10.1017/S1477201908002459.

Maidment, S.C.R., Brassey, C., Barrett, P. M., 2015. The postcranial skeleton of an exceptionally complete individual of the plated dinosaur *Stegosaurus stenops* (Dinosauria: Thyreophora) from the Upper Jurassic Morrison Formation of Wyoming, U.S.A. PLoS One 10, e0138352. https://doi.org/10.1371/journal.pone.0138352.

Maidment, S.C.R., Woodruff, D.C., Horner, J. R., 2018. A new specimen of the ornithischian dinosaur *Hesperosaurus mjosi* from the Upper Jurassic Morrison Formation of Montana, USA, and implications for growth and size in Morrison stegosaurs. J. Vertebr. Paleontol. 38(1), e1406366. https://doi.org/10.1080/02724634.2017.1406366.

Maidment, S.C.R., Raven, T.J., Ouarhache, D., Barrett, P.M., 2020. North Africa's first stegosaur: Implications for Gondwanan thyreophoran dinosaur diversity. Gondwana Res. 77, 82-97. https://doi.org/10.1016/j.gr.2019.07.007.

Maidment, S.C.R., Strachan, S.J., Ouarhache, D., Scheyer, T.M., Brown, E.E., Fernandez, V., Johanson, Z., Raven, T.J., Barrett, P.M., 2021. Bizarre dermal armour suggests the first African ankylosaur. Nat. Ecol. Evol. 5, 1576-1581. https://doi.org/10.1038/s41559-021-01553-6.

Main, R.P., Ricqlès, A. de, Horner, J.R., Padian, K., 2005. The evolution and function of thyreophoran dinosaur scutes: implications for plate function in stegosaurs. Paleobiology 31, 291-314. https://doi.org/10.1666/0094-8373(2005)031[0291:teafot]2.0.co;2.

Mallison, H., 2010. CAD assessment of the posture and range of motion of *Kentrosaurus aethiopicus* Hennig 1915. Swiss J. Geosci. 103(2), 211-233. https://doi.org/10.1007/s00015-010-0024-2.

Marsh, O.C., 1877. New Order of extinct Reptilia (Stegosauria) from the Jurassic of the Rocky Mountains. Am. J. Sci. 3(84), 513-514. https://doi.org/10.2475/ajs.s3-14.84.513.

Mateus, O., Maidment, S.C., Christiansen, N.A., 2009. A new long-necked 'sauropod-mimic' stegosaur and the evolution of the plated dinosaurs. Proc. R. Soc. B: Biol. Sci. 276(1663), 1815-1821. https://doi.org/10.1098/rspb.2008.1909.

Meyer, C.A., Thüring, B., 2004. The first dinosaur footprints from the Middle Jurassic (Bathonian-Callovian) of the Middle Atlas Mountains (Morocco). 2nd Meeting of European Vertebrate Palaeontologist (EAVP). Brno, Abstracts with Programm, p. 20.

Meyer, C.A., Thüring, B., 2005. Mind the "Middle Jurassic" gap. Bone versus track record in dinosaurs. 3rd Swiss Geoscience Meeting, Zurich, pp. 59-60.

Monbaron, M., Russell, D.A., & Taquet, P., 1999. Atlasaurus imelakei ng, n. sp., a brachiosaurid-like sauropod from the Middle Jurassic of Morocco alen. Comptes Rendus de l'Académie des Sciences-Series IIA-Earth and Planetary Science, 329(7), 519-526.

Norman, D.B., 2020. *Scelidosaurus harrisonii* from the Early Jurassic of Dorset, England: the dermal skeleton. Zool. J. Linn. Soc. 190(1), 1-53. https://doi.org/10.1093/zoolinnean/zlz085.

Norman, D.B., 2021. *Scelidosaurus harrisonii* (Dinosauria: Ornithischia) from the Early Jurassic of Dorset, England: biology and phylogenetic relationships. Zool. J. Linn. Soc. 191, 1-86. https://doi.org/10.1093/zoolinnean/zlaa061.

Norman, D.B., Witmer, L.M., Weishampel, D.B., 2004. Basal Thyreophora. In Weishampel, D.B., Dodson, P., Osmólska, H. (eds.), The Dinosauria, second edition. University of California Press, Berkeley, pp. 335-342.

Ostrom, J.H., McIntosh, J.S., 1999. Marsh's Dinosaurs: the collections from Como Bluff. Yale University Press, New Haven, London.

Ouarhache, D., 2002. Sédimentation et volcanismes (effusif et explosif) associés au fifting triasique et infraliasique dans le Moyen Atlas Sud-occidental et la Haute Moulouya (Maroc). Thèse Sci, Univ. Mohamed V, Fac. Sci., Rabat, 282 p.

Ouarhache, D., Charrière, A., Chalot-Prat, F., El Wartiti, M., 2012. Chronologie et modalités du rifting triasico-liasique à la marge sud-ouest de la Téthys alpine (Moyen Atlas et Haute Moulouya, Maroc) ; corrélations avec le rifting atlantique : simultanéité et diachronisme. Bull. Soc. Géol. Fr. 183 (3), 233-249.

Oukassou, M., Zafaty, O., Gierliński, G.D., Klein, H., Saber, H., Amzil, M., Charrière, A., 2023. First record of a small stegosaur footprint (cf. *Stegopodus)* from ?Upper Jurassic-?Lower Cretaceous red beds of the Middle Atlas, Morocco. Ichnos 29(3-4), 195-204. https://doi.org/10.1080/10420940.2023.2182299.

Owen, R., 1842. Report on British fossil reptiles. Part II. In Report of the Eleventh Meeting of the British Association for the Advancement of Science, 1842 (pp. 60-204).

Pratt, J.R., Barbeau, Jr.D.L., Garver, J.I., Emran, A., Izykowski, T.M., 2015. Detrital zircon geochronology of Mesozoic sediments in the Rif and Middle Atlas belts of Morocco: provenance constraints and refinement of the West African signature. J. Geol. 123, 177-200. https://doi.org/10.1086/681218.

Rauhut, O.W.M., Carballido, J.L., Pol, D., 2020. First osteological record of a Stegosaur (Dinosauria, Ornithischia) from the Upper Jurassic of South America. J. Vertebr. Paleontol. 40, e1862133. https://doi.org/10. 1080/ 02724 634.2020.1862133.

Raven, T.J., Maidment, S.C., 2018. The systematic position of the enigmatic thyreophoran dinosaur *Paranthodon africanus*, and the use of basal exemplifiers in phylogenetic analysis. PeerJ 6, e4529. https://doi.org/10.7717/peerj.4529.

Reid, R. E. H., 1996. Bone histology of the Cleveland Lloyd dinosaurs and of dinosaurs in general. Brigham Young Univ. Geol. Stud, 41, 25-71.

Ricqlès, A. de., Pereda-Suberbiola, X.P., Gasparini, Z., Olivero, E., 2001. Histology of dermal ossifications in an ankylosaurian dinosaur from the Late Cretaceous of Antarctica. Publ. Electrón. Asoc. Paleontol. Argent. 7(1), 171-174.

Ridgwell, N., Sereno, P.C., 2010. A basal thyreophoran (Dinosauria, Ornithischia) from the Tiouraren Formation of Niger. In: 70th Annual Meeting of the Society of Vertebrate Paleontology, Pittsburgh, PA. J. Vertebr. Paleontol. 30 (Abstracts Suppl.), pp. 150A-151A.

Riguetti, F.J., Apesteguía, S., Pereda-Suberbiola, X., 2022a. A new Cretaceous thyreophoran from Patagonia supports a South American lineage of armoured dinosaurs. Sci. Rep. 12(1), 11621. https://doi.org/10.1038/s41598-022-15535-6.

Riguetti, F.J., Pereda-Suberbiola, X., Ponce, D., Salgado, L., Apesteguía, S., Rozadilla, S., Arbour, V., 2022b. A new small-bodied ankylosaurian dinosaur from the Upper Cretaceous of North Patagonia (Río Negro Province, Argentina). J. Syst. Palaeontol. 20(1), 2137441. https://doi.org/10.1080/14772019.2022.2137441.

Scheyer, T., Sander, P.M., 2004. Histology of ankylosaur osteoderms: implications for systematics and function. J. Vertebr. Paleontol. 24, 874-893. https://doi.org/10.1671/0272-4634(2004)024[0874:HOAOIF]2.0.CO;2

Seeley, H.G., 1888. I. On the classification of the fossil animals commonly named Dinosauria. Proceedings of the Royal Society of London, *43*(258-265), 165-171.

Sereno, P.C., Dong, Z.M., 1992. The skull of the basal stegosaur *Huayangosaurus taibaii* and a cladistic diagnosis of Stegosauria. J. Vertebr. Paleontol. 12, 318–343. https://doi.org/10.1080/02724634.1992.10011463.

Soto-Acuña, S., Vargas, A.O., Kaluza, J., Leppe, M.A., Botelho, J.F., Palma-Liberona, J., and Rubilar-Rogers, D., 2021. Bizarre tail weaponry in a transitional ankylosaur from subantarctic Chile. Nature 600(7888), 259-263. https://doi.org/10.1038/s41586-021-04147-1

Termier, H., 1936. Études géologiques sur le Maroc central et le Moyen-Atlas méridional. Notes et Mémoires du Service de Mines Carte géologique Maroc, 33, 1-743.

Termier, H., Gubler, J., de Lapparent, A.F., 1940. Le Bathonien de la région d'El Mers : Reptiles et poisons du Bathonien d'El Mers. C. R. Hebd. Séances Acad. Sci. 210, 768-770.

Upchurch, P., Martin, J., 2003. The anatomy and taxonomy of *Cetiosaurus* (Saurischia, Sauropoda) from the Middle Jurassic of England. J. Vertebr. Paleontol. 23(1), 208-231. https://doi.org/10.1671/0272-4634(2003)23%5B208%3ATAATOC%5D2.0.CO%3B2.

Vianey-Liaud, M., Garcia, G., 2003. Diversity among North Africa Dinosaur eggshell. Palaeovertebrata 32, 171-188.

Vickaryous, M.K., Hall, B.K., 2008. Development of the dermal skeleton in *Alligator mississippiensis* (Archosauria, Crocodylia) with comments on the homology of osteoderms. J. Morphol. 269, 398-422.

Wilson, J.A., 1999. A nomenclature for vertebral laminae in sauropods and other saurischian dinosaurs. J. Vertebr. Paleontol. 19(4), 639-653. https://doi.org/10.1080/02724634.1999.10011178.

Wolf, D., Kalthoff, D.C., Sander, P.M., 2012. Osteoderm histology of the Pampatheriidae (Cingulata, Xenarthra, Mammalia): implications for systematics, osteoderm growth, and biomechanical adaptation. J. Morphol. 273, 388-404. https://doi.org/10.1002/jmor.11029.

Zafaty, O., Oukassou, M., Si Mhamdi, H., Tabuce, R., Charrière, A., 2023. Integrated remote sensing data and field investigations for geological mapping and structural analysis. The case of SW Tichoukt ridge (Middle Atlas, Morocco). J. Afr. Earth Sci. 198, 104784. https://doi.org/10.1016/j.jafrearsci.2022.104784.

Zhou, S.-W., 1984. The Middle Jurassic dinosaurian fauna from Dashanpu, Zigong, Sichuan, vol. 2: Stegosaurs. Sichuan Scientific and Technological Publishing House, Sichuan, 51 pp. [Chinese, 1–45; English, 45–51].

Fig. 1. Location of the HIIUC BN fossil site. (A) Geographical map of Morocco. (B) Simplified structural map of the central Middle Atlas. (C) Geological map of the Boulemane area in the Middle Atlas (simplified after Zafaty et al., 2023). NMAFZ: Northern Middle Atlas Fault Zone; MAFZ: Middle Atlas Fault Zone; SMAFZ: Southern Middle Atlas Fault Zone.

Fig. 2. (A) Stratigraphic succession and sedimentary facies of the Boulahfa north fossil site (Morocco). (B) Panoramic view of the Jurassic ?Cretaceous deposits at the HIIUCBN fossil site. (C) Erosional disconformity (paleochannel) between the El Mers III Formation and Oued El Atchane Formation. (D) Soft sediment deformation of versicolor laminated marls in the basal part of the section related to sauropod walking. (E) Sauropod footprint. (F) Fossil wood associated with HIIUC BN. (G) Rhizolites at the base of the Oued El Atchane Formation. (H) Isolated stegosaurian dermal element.

Fig. 3. (A) Panoramic view of the northern Boulahfa fossil site (Morocco). (B) Quany map drawn during the excavation of HIIUC BN. (C D) Excavation process and site evolution. (E J) fossil specimens in situ taken at different times during the excavation.

Fig. 4. HIIUC BN, holotype specimen of *Thyreosaurus* atlasicus gen. et sp. nov. from the Middle Jurassic (Bathonian-?Callovian) of Morocco. Dorsal vertebrae (A) HIIUC BN05, (B) HIIUC BN06, and (C) HIIUC BN04, in anterior (a), left lateral (b), posterior (c), right lateral (d), dorsal (e), and ventral (f) views. 3D models (a' f'). Abbreviations: cm, centrum; dia, diapophysis; ipzs, intraprezygapophyseal shelf; foss, fossa; k, keel; nc, neural canal; mr, midline ridge; ns, neural spine; para, parapophysis; poz, postzygapophysis; prz, prezygapophysis; ri, ridge. Scale bar = 5 cm.

Fig. 5. HIIUC BN, holotype specimen of *Thyreosaurus* atlasicus gen. et sp. nov. from the Middle Jurassic (Bathonian-?Callovian) of Morocco. Dorsal vertebrae (A) HIIUC BN01 and (B) HIIUC BN02, in anterior (a), left lateral (b), posterior (c), right lateral (d), dorsal (e), and ventral (f) views. 3D models (a' f'). Abbreviations: cm, centrum; dia, diapophysis; foss, fossa; k, keel; mr, midline ridge; nc, neural canal; ns, neural spine; para, parapophysis; poz, postzygapophysis; prz, prezygapophysis; ri, ridge; tp, transverse processes. Scale bar = 5 cm.

Fig. 6. HIIUC BN, holotype specimen of *Thyreosaurus* atlasicus gen. et sp. nov. from the Middle Jurassic (Bathonian-?Callovian) of Morocco. Dorsal vertebrae (A) HIIUC BN03, (B) HIIUC BN07, and (C) HIIUC BN08, in anterior (a), left lateral (b), posterior (c), right lateral (d), dorsal (e), and ventral (f) views. 3D models (a' f'). Abbreviations: cm, centrum; dia, diapophysis; foss, fossa; k, keel; mr, midline ridge; nc, neural canal; ns, neural spine; para, parapophysis; poz, postzygapophysis; prz, prezygapophysis; ri, ridge. Scale bar = 5 cm.

Fig. 7. HIIUC BN, holotype specimen of *Thyreosaurus* atlasicus gen. et sp. nov. from the Middle Jurassic (Bathonian-?Callovian) of Morocco. HIIUC BN dorsal ribs in anterior and posterior views. (A) HIIUC BN18 (left dorsal rib), (B) HIIUC BN19, (C) HIIUC BN20, (D) HIIUC BN21, (E) HIIUC BN22, (F) HIIUC BN23, (G) HIIUC BN24 (right dorsal ribs). 3D models (A0 –G0). Abbreviations: cp: capitulum; tb: tuberculum. Scale bar = 10 cm.

Fig. 8. HIIUC BN, holotype specimen of *Thyreosaurus* atlasicus gen. et sp. nov. from the Middle Jurassic (Bathonian-?Callovian) of Morocco. HIIUC BN11 osteoderm in ventral (A) and dorsal (B) views; natural edges (C E); incomplete edges (D F). 3D models (A0 –F0). Scale bar = 10 cm.

Fig. 9. HIIUC BN, holotype specimen of *Thyreosaurus* atlasicus gen. et sp. nov. from the Middle Jurassic (Bathonian-?Callovian) of Morocco. (A) HIIUC BN12 osteoderm in ventral (b) and dorsal (d) views; incomplete edges (a, c, e); natural edge (f). (B) HIIUC BN13 osteoderm in ventral (b) and dorsal (d) views; natural edges (a, c, e, f). (C) HIIUCBN16 osteoderm in dorsal (b) and ventral (d) views; natural edges (a, c). 3D models in prime letters (a0 –f0). Scale bar = 5 cm.

Fig. 10. Bane histology of *Thyreosaurus* atlasicus gen. et sp. nov. osteoderms from the Middle jurassic (Bathonian-? Callovian) of Morocco. (A) Images of the sampled specimens HIIUC BN14 and HIIUC BN15 with enlargement of the sectioned area. Red !ines indicate the planes of sectioning. Dashed line indicates the boundary between the osteoderm cortex and interna!core. (B) Detailed view of the ornamented surface of the osteoderms (yellow box inset in A), consisting of cross hatching ossified collagen fibers at angles between 90° and 110°. (C) Vertical thin section of the osteoderm HIIUC BN14 showing the extensive secondary remodeling that reaches the external surface and obliterates most of the primary tissues. (D) Detail of the outermost cortex of the osteoderm HIIUCBN15. Near the periphery, the primary bane tissue is composed of interwoven structural liber bundles. The remainder of the cortex consists of bath Haversian (overlapping secondary osteons) and thiel< trabecular bane (large resorption cavities lined by lam ella te layers). Sorne interstitial primary bane is also visible (white

arrows). The dashed line marks the progress of the secondary remodeling. (E) Detail of the external cortex of the osteoderm HIIIUC BN15 showing the arrangement of three orthogonal systems of structural fiber bundles. Note the presence of a vertical foramen sectioned longitudinally in the center of the image. Abbreviations: HBF, horizontal liber bundles. HC, Haversian canals. !PB, interstitial primary bane. PWC, primary woven bane. RS, resorption room. SRB, secondary remodeled bane. SF, structural libers. 50, secondary osteons. SVC, simple vascular canals. THBF, transversely sectioned horizontal liber bundles. VBF, vertical liber bundles. Pictures taken in plane polarized light (PPL). Scale bars in figures B E1 mm. (For interpretation of the references to colour in this figure legend, the reader is referred to the web version of this article.)

Fig. 11. Bone histology of *Thyreosaurus* atlasicus gen. et sp. nov. dorsal rib from the Middle Jurassic (Bathonian-? Callovian) of Morocco. (A) Overall transverse section of the dorsal rib HIIUC BN25 showing the general bone structure. Yellow inset box indicates the position of magnified figure B. (B) General view of the middle and outer cortex (box inset in A) showing a well vascularized zonal bone tissue. Note the presence of at least six LAGs (white arrowheads) which appear as simple or multiple rest lines, counted here as single events. Note the extensive secondary remodeling (Haversian bone) in the internal (i.e., older) cortex. Abbreviations: CVC, circular vascular canal. LVC, longitudinal vascular canal. SO, secondary osteons. Scale bar = 1 cm in A and 1 mm in B. (For interpretation of the references to colour in this figure legend, the reader is referred to the web version of this article.)

Fig. 12. Time calibrated strict consensus of one MPT (L = 269.67). Branch supports are figured in each node (Bootstrap/Symmetrical resampling). The age of each record was taken from Arbour and Currie (2016), Maidment et al. (2020), Norman (2021) and Dai et al. (2022).

Table 1
List and measurements taken on the material of *Thyreosaurus* atlasicus in mm (*: measurements made on incomplete elements).

IBERIA
ALBORAN SEA
Rabat
Fez
Marrakech
Agadir
ATLANTIC OCEAN
MOROCCO
ALGERIA
MAURITANIA
500 km
A
10°W
0°
30°N
20°N
5°W
N4
N13
TICHOUKT RIDGE
TABULAR MIDDLE ATLAS
Boulemane
Fig. 1C
NMAFZ
MAFZ
SMAFZ
FOLDED MIDDLE ATLAS
HIGH MOULOUYA
10 km
33°N
B

Quaternary alluviums
Plio-quaternary basalts
Pliocene
Eocene
Upper Cretaceous
Lower Cretaceous
Angular unconformity
?Upper Jurassic-?Lower Cretaceous
Erosional disconformity
Bathonian-?Callovian
Bajocian
Liassic
Triassic
Fault
Thrust Fault
Main road
Track
River
Localities
Alluvial fan
HIIUC-BN Fossil site

4°50'W
Almis Guigou
4°40'W
TICHOUKT
Oued Guigou
Jbel Tajda
38°20'N
Boulemane
Boulahfa North
Boulahfa quarry
33°20'N
AIN NOKRA SYNCLINE
OUDIKSOU SYNCLINE
EL MERS SYNCLINE
Jbel Oudiksou
Saf
Aït Karmous
Anjil Ikhatarn
Jbel Ighounba
Jbel Qarbous
Jbel Abbou
33°15'N
Achlouj
Tapuirt Tamqrant
33°10'N
N
W
E
S
5 km
C
5°W
4°50'W
4°40'W

A

?Upper Jurassic - ?Lower Cretaceous

Oued El Atchane Fm.

30m

r

r

r

g

r

r

g

r

g

?Bathonian - ?Callovian

El Mers III Fm.

10m

B

Oued El Atchane Fm.

El Mers III Fm.

C

D

E

Manus

Pes

F

G

H

Dolomitic limestones

Marls, silts (**r**:red; **g**: green)

Sandstones

Conglomerates

Erosional disconformity

Planar Horizontal lamination

Planar cross lamination

Cross bedding

HIIUC-BN Fossil site

Ripple marks

Bioturbation

Rhizolites

Pyrite concretions

Fossil wood

Dinosaur bones

Sauropod footprint

Stegosaur footprint


Oued El Atchane Fm.
HIIUC-BN Fossil site
Erosional disconformity
El Mers III Fm.
A

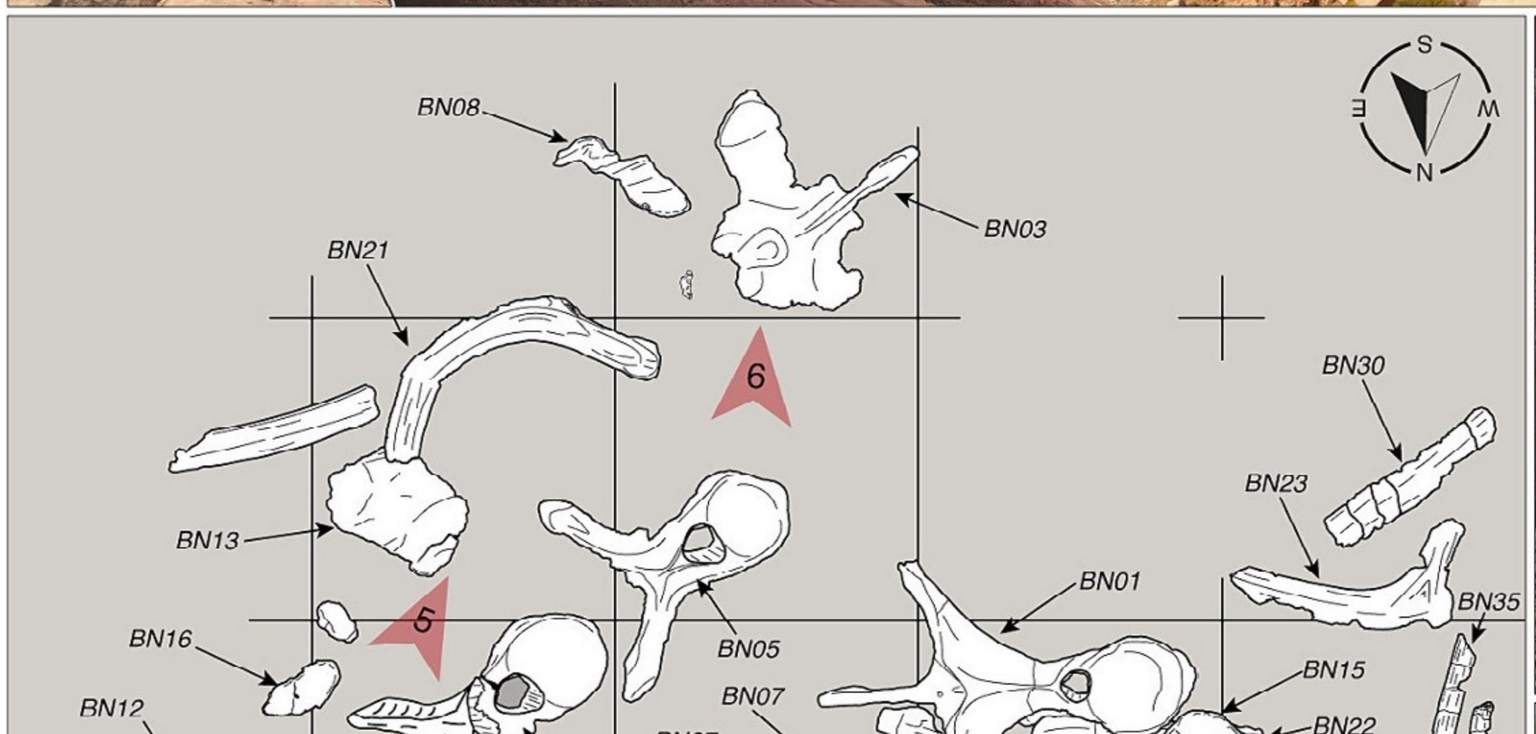
BN08
BN03
BN21
6
BN30
BN23
BN13
BN01
BN35
5
BN16
BN05
BN15
BN12
BN07
BN22
BN27
BN06
BN25
BN31
4
BN34
BN38
BN37
BN39
BN33
BN18
BN36
BN19
BN26
BN32
2
BN28
BN24
BN29
BN20
BN11
1
BN02
3
BN14
BN04
Excavation progress direction
B
20 cm

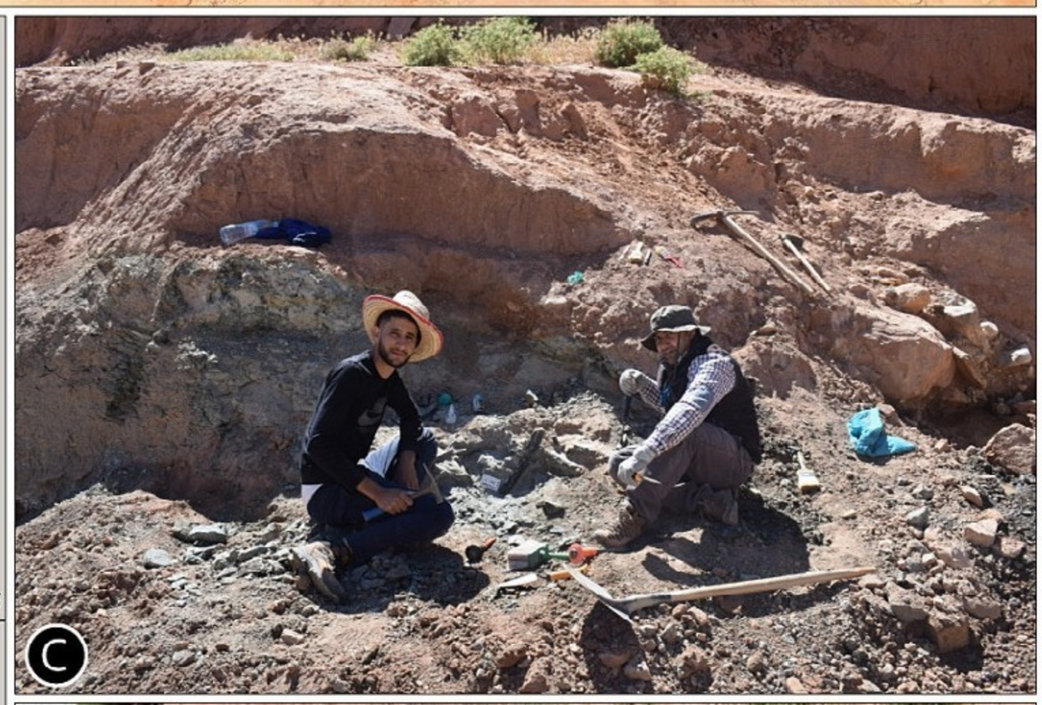
C
D

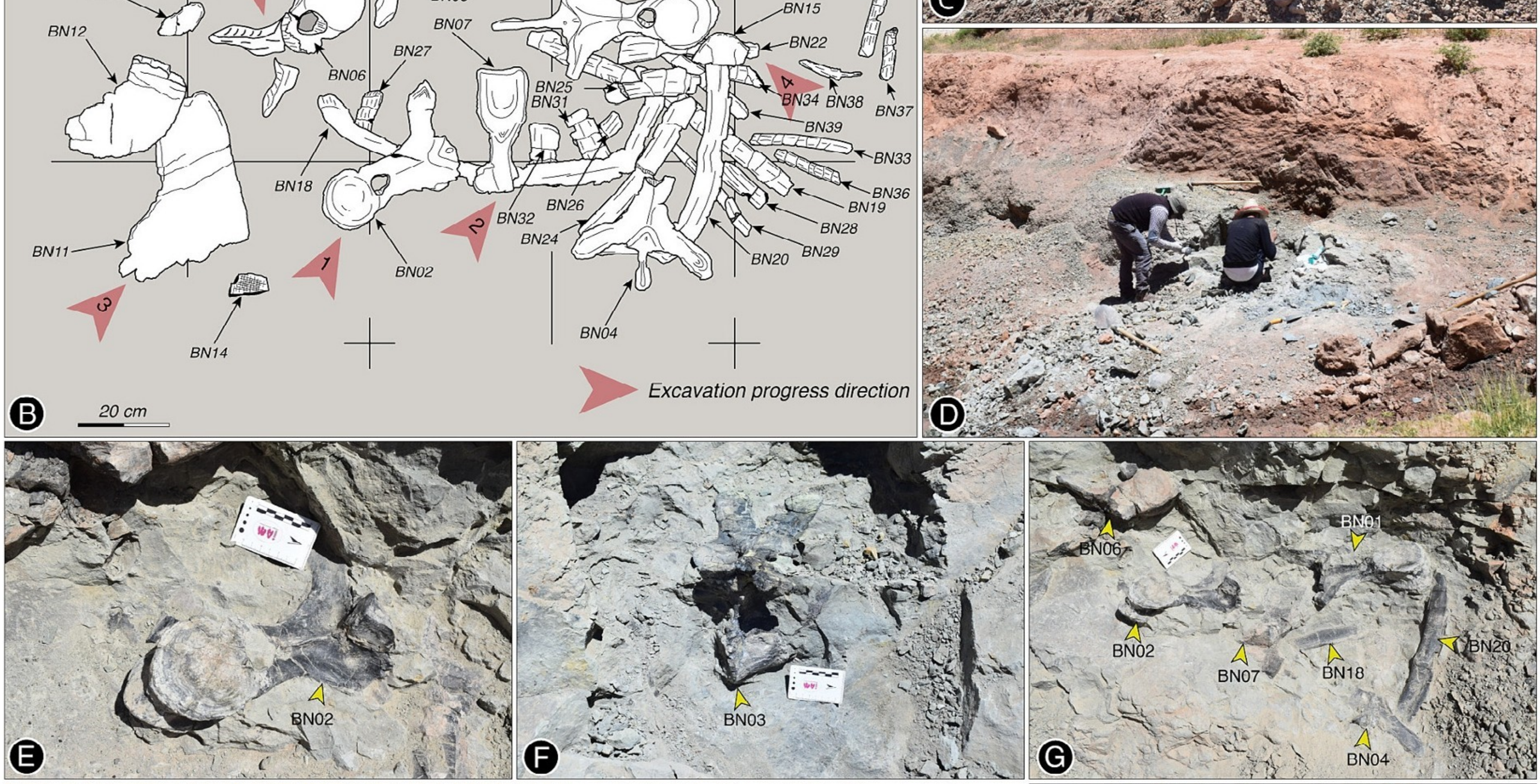
BN02
E
BN03
F
BN06
BN01
BN02
BN07
BN18
BN20
BN04
G


BN22
BN18
BN20
H
BN11
I
BN21
BN13
J

A

a

b

c

d

e

f

prz
foss
nc
cm
dia
prz
para
ri
nc
cm
dia
para
ri
e'
prz
a'
b'
c'
d'
f'
k

B

a

b

c

d

e

f

nc
cm
nc
cm
a'
b'
c'
d'
e'
f'
k

C

a

b

c

d

e

f

ns
prz
mr
foss
ns
dia
ns
poz
foss
ri
dia
poz
poz
e'
ns
a'
b'
c'
d'
f'

A

a

b

c

d

e

f

ns

prz

mr

foss

nc

cm

ri

poz

tp

dia

para

k

a'

b'

c'

d'

e'

f'

B

a

b

c

d

e

f

ns

mr

prz

foss

nc

cm

dia

ri

poz

tp

para

k

a'

b'

c'

d'

e'

f'

A

a

b

c

d

e

f

ns
mr
prz
foss
nc
cm
a'

prz
ns
ri
b'

poz
tp
foss
nc
cm
c'

dia
prz
poz
para
ri
d'

ns
foss
ipzs
prz
e'

f'
k

B

a

b

c

d

e

f

tp
prz
nc
cm
a'

prz
tp
para
b'

tp
nc
cm
c'

prz
d'

e'
prz

f'
k

C

a

b

c

d

e

f

ns
a'

ns
poz
b'

poz
c'

d'

e'
ns
poz
f'


A
B
C
D
E
F
G
A’
B’
C’
cp
tb
D’
E’
cp
tb
F’
cp
tb
G’


E
C
A
D
B
F
E'
C'
A'
D'
B'
F'

A

a

b

c

d

e

f

a'

b'

c'

d'

e'

f'

B

a

b

c

d

e

f

a'

b'

c'

d'

e'

f'

C

a

b

c

d

a'

b'

c'

d'

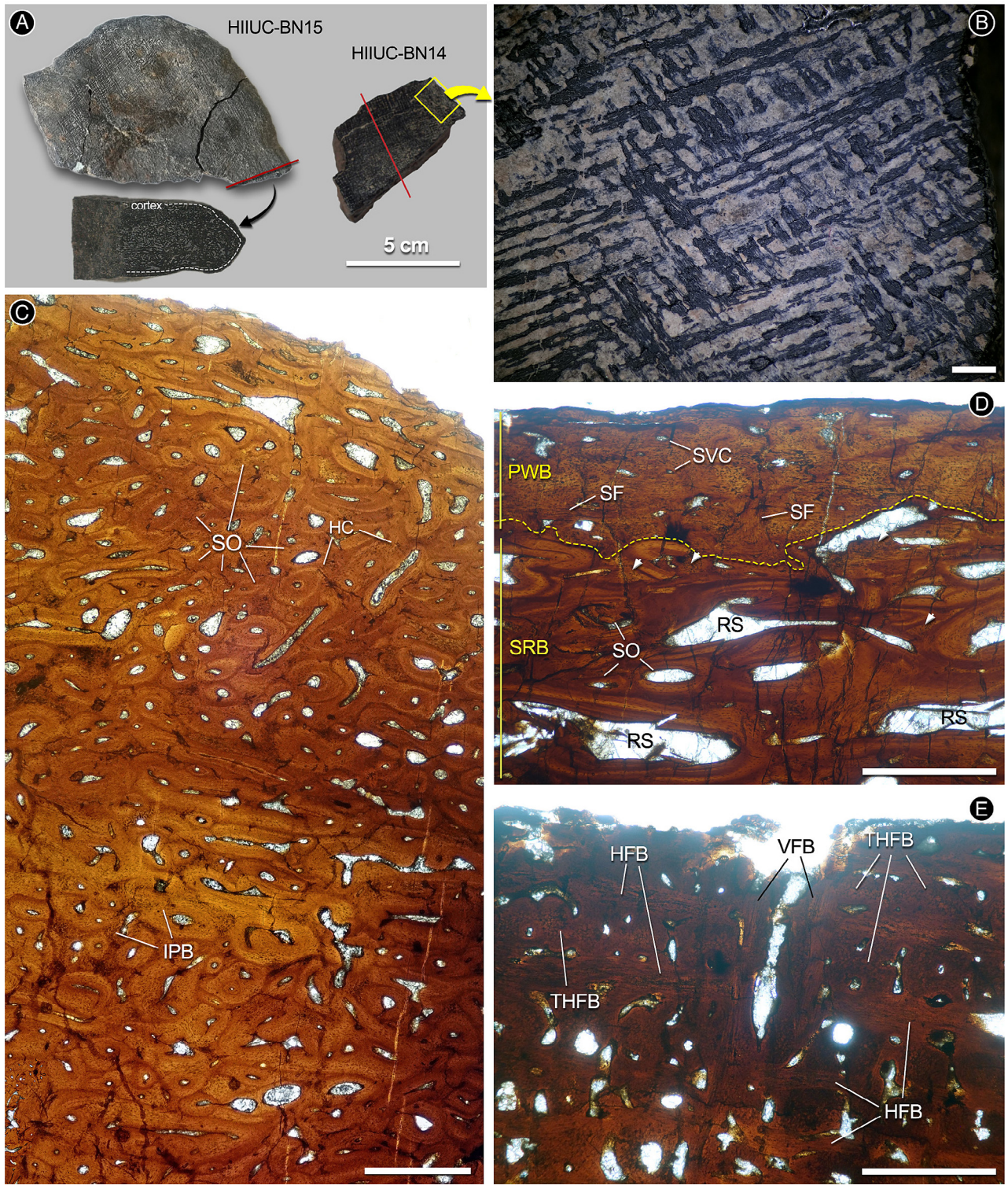
A
HIIUC-BN15
HIIUC-BN14
cortex
5 cm
B
C
SO
HC
IPB
D
PWB
SVC
SF
SF
RS
SRB
SO
RS
RS
E
HFB
VFB
THFB
THFB
HFB

A

B

CVC

LVC

SO

SO

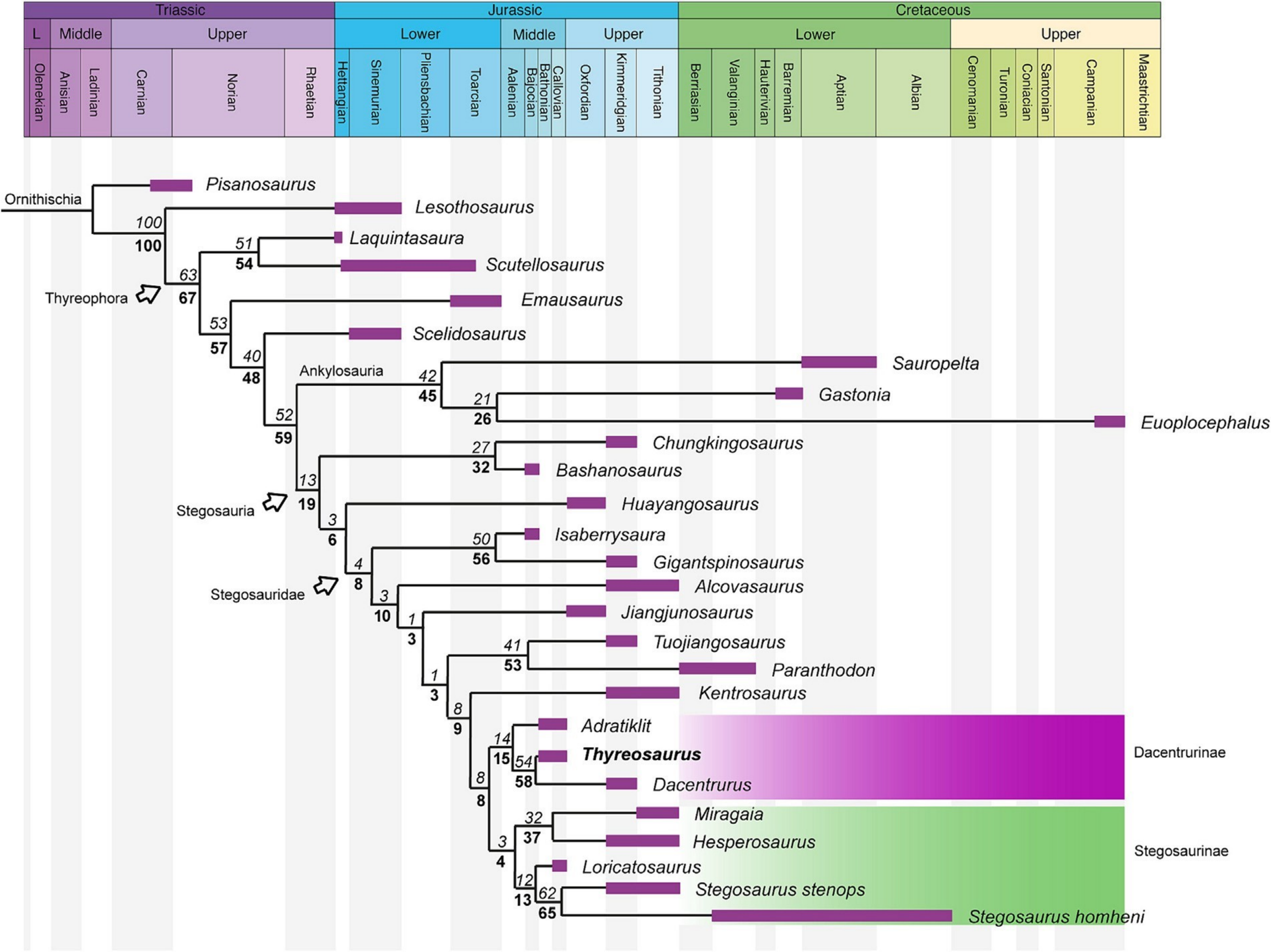
Triassic
Jurassic
Cretaceous
L
Middle
Upper
Lower
Middle
Upper
Lower
Upper
Olenekian
Anisian
Ladinian
Carnian
Norian
Rhaetian
Hettangian
Sinemurian
Pliensbachian
Toarcian
Aalenian
Bajocian
Bathonian
Callovian
Oxfordian
Kimmeridgian
Tithonian
Berriasian
Valanginian
Hauterivian
Barremian
Aptian
Albian
Cenomanian
Turonian
Coniacian
Santonian
Campanian
Maastrichtian
Ornithischia
Pisanosaurus
Lesothosaurus
Laquintasaura
Scutellosaurus
Thyreophora
Emausaurus
Scelidosaurus
Ankylosauria
Sauropelta
Gastonia
Euoplocephalus
Chungkingosaurus
Bashanosaurus
Stegosauria
Huayangosaurus
Isaberrysaura
Gigantspinosaurus
Stegosauridae
Alcovasaurus
Jiangjunosaurus
Tuojiangosaurus
Paranthodon
Kentrosaurus
Adratiklit
Thyreosaurus
Dacentrurus
Dacentrurinae
Miragaia
Hesperosaurus
Loricatosaurus
Stegosaurus stenops
Stegosaurus homheni
Stegosaurinae
100
100
51
54
63
67
53
57
40
48
52
59
42
45
21
26
27
32
13
19
3
6
50
56
4
8
3
10
1
3
41
53
1
3
8
9
14
15
54
58
8
8
32
37
3
4
12
13
62
65

Table 1
List and measurements taken on the material of *Thyreosaurus atlasicus* in mm (*: measurements made on incomplete elements).

Dorsal vertebrae

		Centrum length	Anterior articular facet width	Anterior articular facet height	Posterior articular facet width	Posterior articular facet height	Neural arch height	Neural spine height	Neural spine length	Neural canal height (measured anteriorly)	Neural canal width (measured anteriorly)	Neural canal height (measured posteriorly)	Neural canal width (measured posteriorly)
HIIUC-BN01	centrum, neural arch (diapophyses and neural spine)	80	107	100	100	110	235	105	53	48	37	36	35
HIIUC-BN02	centrum+neural arch (one diapophysis, broken neural spine)	71	95	91	96	93	170*	-	58*	53	37	38	38
HIIUC-BN03	centrum+neural arch (diapophyses and neural spine)	104	95	86	94	72	115	90	63	26	18	26	24
HIIUC-BN04	neural arch (diapophyses and neural spine)	-	-	-	-	-	210	89	65	-	-	-	-
HIIUC-BN05	centrum+neural arch (diapophyses)	78	99	92	107	86	82*	-	-	46	44	45	41
HIIUC-BN06	centrum+basal part of neural arch	85	96	94	114	95	-	-	-	45	41	47	42
HIIUC-BN07	centrum+neural arch (broken diapophyses)	99	65	97	63	95	113*	-	-	39	16	33	21
HIIUC-BN08	neural arch (neural spine)	-	-	-	-	-	-	102	72	-	-	-	-
HIIUC-BN09	fragmentary centrum+basal part of the neural arch	80		83		72							

Osteoderms

		Maximum length	Maximum width	Maximum thickness	Minimum thickness
HIIUC-BN11	large osteoderm	317	270	34	17
HIIUC-BN12	large osteoderm	259	152	50	22
HIIUC-BN13	Osteoderm	170	122	24	8
HIIUC-BN14	osteoderm (sample for histology)				
HIIUC-BN15	osteoderm (sample for histology)				
HIIUC-BN16	small osteoderm	89	48	17	3

Fibula?

		Total length
HIIUC-BN39	long incomplete bone (fibula?)	258*

Dorsal ribs

		Total length	Capitulum length	Tuberculum length
HIIUC-BN18	dorsal rib	645*	15	60
HIIUC-BN19	fragment of dorsal rib	571*	-	-
HIIUC-BN20	dorsal rib	478*	30	117
HIIUC-BN21	dorsal rib in two fragments	500*	27	120
HIIUC-BN22	proximal part of dorsal rib	300*	42	96
HIIUC-BN23	proximal part of dorsal rib	280*	54	86
HIIUC-BN24	fragment of dorsal rib	371*	-	-
HIIUC-BN25	proximal fragment of dorsal rib (sample for histology)	185*		
HIIUC-BN26	tuberculum			105
HIIUC-BN27	tuberculum			115
HIIUC-BN28	fragment of dorsal rib	99*		
HIIUC-BN29	distal part? of dorsal rib	248*		
HIIUC-BN30	distal part? of dorsal rib	244*		
HIIUC-BN31	distal part? of dorsal rib	121*		
HIIUC-BN32	distal part? of dorsal rib	92*		
HIIUC-BN33	fragment of dorsal rib	234*		
HIIUC-BN34	fragment of dorsal rib	216*		
HIIUC-BN35	fragment of dorsal rib	157*		
HIIUC-BN36	fragment of dorsal rib	158*		
HIIUC-BN37	fragment of dorsal rib	118*		
HIIUC-BN38	distal part? of dorsal rib	136*		